REPORT DOCUMENTATION PAGE

Form Approved
OMB No. 0704-0188

1. REPORT DATE *(DD-MM-YYYY)*	2. REPORT TYPE	3. DATES COVERED *(From - To)*
09-02-2010	FINAL	Apr 2007 - Feb 2010

4. TITLE AND SUBTITLE

THIN FILMS OF REDUCED HAFNIUM OXIDE WITH EXCESS CARBON FOR HIGH-TEMPERATURE OXIDATION PROTECTION

5a. CONTRACT NUMBER
FA9550-07-C-0046

5b. GRANT NUMBER

5c. PROGRAM ELEMENT NUMBER

6. AUTHOR(S)

Dusan A. Pejakovic, Ph.D.

5d. PROJECT NUMBER

5e. TASK NUMBER

5f. WORK UNIT NUMBER

7. PERFORMING ORGANIZATION NAME(S) AND ADDRESS(ES)

SRI International
333 Ravenswood Ave.
Menlo Park, CA 94025

8. PERFORMING ORGANIZATION REPORT NUMBER

MP 10-004

9. SPONSORING / MONITORING AGENCY NAME(S) AND ADDRESS(ES)

Air Force Office of Scientific Research
Directorate of Aerospace, Chemistry and Material Sciences
875 North Randolph Street
Suite 325, Room 3112
Arlington, Virginia 22203

10. SPONSOR/MONITOR'S ACRONYM(S)
AFOSR

11. SPONSOR/MONITOR'S REPORT NUMBER(S)

12. DISTRIBUTION / AVAILABILITY STATEMENT

Distribution Statement A. Approved for public release; distribution is unlimited or as the Contracting Officer suggested (publicly releasable).

13. SUPPLEMENTARY NOTES

14. ABSTRACT

The overall objective of the project was to achieve controlled synthesis of carbon-rich hafnia, HfO_xC_y, and investigate the fundamental and high-temperature properties of this material. HfO_xC_y is normally formed as a compact and pore-free oxide interlayer during oxidation of hafnium carbide (HfC), where it acts as the primary oxygen diffusion barrier. Pulsed laser deposition (PLD) was used to establish routes for direct synthesis of films in the HfO_xC_y system. High-quality films with high carbon contents were synthesized using pure HfO_2 pellets as PLD targets and acetylene (C_2H_2) gas as a source of carbon. Post-deposition annealing was used to reduce the hydrogen content in the films and increase sp^2 bonding of carbon. Comprehensive characterization of the films was performed using a variety of analytical methods, and it was established that the films represent close analogs of the HfO_xC_y interlayer oxides, with elemental carbon dispersed in an amorphous HfO_2 matrix on a length scale smaller than 5 nm. It was shown that high carbon content in the films inhibits crystallization of HfO_2 at temperatures at least up to 900 °C. Study of the diffusion of ^{18}O-enriched oxygen in the films indicated that the oxygen diffusivity is considerably lower in amorphous C-rich layers than in microcrystalline C-depleted layers. Treatment of the films in oxidizing environments at temperatures above 550 °C leads to a rapid loss of carbon and crystallization of HfO_2.

15. SUBJECT TERMS
High-temperature properties, hypersonics, oxidation protection, ceramics, hafnia, hafnium carbide, carbon, films

16. SECURITY CLASSIFICATION OF:			17. LIMITATION OF ABSTRACT	18. NUMBER OF PAGES	19a. NAME OF RESPONSIBLE PERSON
a. REPORT	b. ABSTRACT	c. THIS PAGE			Dusan A. Pejakovic, Ph.D.
U	UU		SAR	30	19b. TELEPHONE NUMBER *(include area code)* (650) 859-5129

Final Performance Report • February 2010

Thin Films of Reduced Hafnium Oxide with Excess Carbon for High-Temperature Oxidation Protection

AFOSR Contract No. FA9550-07-C-0046
SRI Project No. P17935
SRI Report No. MP 10-004
Period of Performance: 04/15/2007–11/30/2009

Principal Investigator: Dr. Dušan Pejaković
Molecular Physics Laboratory, SRI International

Prepared for:
Dr. Joan Fuller
Director, High Temperature Aerospace Materials Program
AFOSR/NA
801 North Randolph Street, Room 732
Arlington, VA 22203-1977

Approved by:
Richard Copeland, Director
Molecular Physics Laboratory, SRI International

333 Ravenswood Avenue • Menlo Park, California 94025-3493 • 650.859.2000 • www.sri.com

INTRODUCTION

This report summarizes the activities and results of experimental work performed for the Air Force Office of Scientific Research (AFOSR) under Contract FA9550-07-C-0046, "Thin Films of Reduced Hafnium Oxide with Excess Carbon for High-Temperature Oxidation Protection." The overall objective of this 3-year project was to achieve controlled synthesis of carbon-rich hafnia, $HfO_{2-x}C_y$, and investigate the fundamental and high-temperature properties of this material. $HfO_{2-x}C_y$ is naturally formed as a compact and pore-free oxide interlayer during oxidation of hafnium carbide (HfC), where it is though to act as a primary oxygen diffusion barrier. The specific project goals were to: 1) use pulsed laser deposition (PLD) to establish routes for direct synthesis of films in the $HfO_{2-x}C_y$ system; 2) investigate high-temperature oxygen diffusion in $HfO_{2-x}C_y$ films; and 3) evaluate the potential of $HfO_{2-x}C_y$ films for high-temperature oxidation protection coatings. As an additional activity in the third project year, we investigated the correlation between the luminescent properties and microstructure of HfO_2 in the bulk and thin film forms. The results of this research have led to four presentations at conferences and professional meetings and two peer-reviewed journal papers. One further manuscript is under preparation. Research efforts and accomplishments are summarized below.

SUMMARY OF EFFORTS AND ACCOMPLISHMENTS

Overview of accomplishments

SRI International (SRI) developed two PLD-based synthesis routes to carbon-rich hafnia. The more functional of these two routes (using pure HfO_2 PLD targets and acetylene gas as the source of carbon) was then investigated in detail, and films with a broad range of carbon fractions were deposited on different substrates. Stable films up to 700 nm thick and with high molar fractions (~0.1–0.45) of carbon were obtained. Post-deposition annealing (PDA) at a relatively low temperature of 600 °C was used to reduce the content of hydrogenated carbon and enhance the sp^2 carbon-carbon bonding. The films were characterized using the analytical techniques of scanning electron microscopy (SEM), transmission electron microscopy (TEM), energy dispersive spectroscopy (EDS) in both SEM and TEM, X-ray photoelectron spectroscopy (XPS), Rutherford backscattering spectroscopy (RBS), hydrogen forward scattering (HFS), Raman spectroscopy (RS), X-ray diffraction (XRD), and depth profiling by secondary-ion mass spectroscopy (SIMS). Based on this comprehensive sample characterization, it is established that, following PDA, the films represent a close analog of the carbon-rich hafnia interlayer that forms in oxidized HfC, with elemental carbon dispersed in an amorphous HfO_2 matrix on a length scale smaller than 5 nm. We investigated crystallization of films upon annealing at temperatures up to 900 °C, and found that high molar fractions of carbon inhibit long-range crystallization of HfO_2. Study of the diffusion of ^{18}O-enriched oxygen in the films indicated that the oxygen diffusivity is considerably lower in amorphous C-rich layers than in microcrystalline C-depleted layers. Oxidation studies of the films showed that at temperatures above 550 °C and at low O_2 pressures a rapid loss of carbon occurs, accompanied by crystallization of HfO_2.

The project benefited from the collaboration with Prof. Bridget Rogers (Vanderbilt University), whose research group performed RBS and XPS analyses of selected films synthesized at SRI International (SRI). In addition, a graduate student from Prof. Rogers' group,

Mekha George, spent about 10 months at SRI in the first project year performing PLD synthesis under the supervision of the PI, Dr. Pejaković. During the third year of the project, Dr. Pejakovic established collaboration with Evans Analytical Group (EAG) in Sunnyvale, CA. EAG scientists performed some state-of-the-art analyses of the thin-film samples, including TEM, XPS, Raman spectroscopy, SIMS, and RBS/HFS analysis.

Experimental methodology

PLD was performed at room temperature in a stainless steel vacuum chamber evacuated by a turbomolecular pump, backed by a dry scroll pump. The chamber was fitted with a heated sample holder (temperature up to 900 °C), acquired and installed during the first project year. For one of the synthesis routes used, a continuous flow of C_2H_2 (99.6% purity, dissolved in acetone) was introduced into the chamber after reaching base pressure of about 7×10^{-5} Pa. The flow rate of C_2H_2 was regulated by an electronic mass flow controller, and the C_2H_2 pressure was measured by a capacitance pressure gauge. Following PLD, substrates with films were cleaved into 2-3 parts and some of them were subjected to post-deposition thermal treatment. PDA was performed either in a tube furnace with a continuous flow of gas (oxidation studies), or in the PLD chamber itself (annealing in vacuo). In the latter case, silver paint was used to attach the substrates to the heater.

Pure sintered HfO_2 tablets with a nominal purity of 99.9%[4] were acquired from Cerac, Inc. and used as PLD targets. The HfO_2/graphite targets (see below) were produced using materials acquired from Cerac as well. The targets were rotated at a rate of 20-30 rpm during film deposition. Silicon substrates were cleaved from an n-type Si(001) wafer. HOPG substrates were acquired from SPI Supplies, Inc. The target-substrate distance was usually 5 cm.

Ablation of HfO_2 targets was performed using a XeCl excimer laser, which provided ~15 ns long pulses at a wavelength of 308 nm. The laser beam was tightly focused by a spherical lens onto the target at a 45° incident angle to achieve a fluence of about 3 J/cm^2. Prior to film deposition, the substrate was shielded by a movable shutter and target was pre-ablated for 10 min to remove any contamination from target surface. The laser was operated at a repetition rate of 2 Hz and the film growth rate was found to be on the order of 0.1 Å/pulse.

The XPS analysis was performed using a PHI Quantum 2000 instrument equipped with a Monochromated Al-K_α source ($h\nu$ = 1486.6 eV). The analysis area was 1.4×0.3 mm. A large take-off angle (TOA) of 75° was used to maximize the depth of photoelectron detection and thus minimize the contribution of surface contaminants to the data.

The Raman spectra were collected on a Jobin Yvon LABRAM spectrometer equipped with an Olympus BX40 microscope using the backscattering geometry. An Ar^+ ion laser (514.5 nm wavelength) and a grating with 1800 gr/mm were used in these measurements. The probe spot size was 1-2 μm. For each analyzed sample, the Raman spectra were collected for at least 3 different surface sites. No significant variation of the spectra with position was observed, except for the samples grown in 0.08 Pa of C_2H_2, as will be discussed below.

RBS was performed using He^{++} ion beam with energy of 2.275 MeV. The incident ion trajectory was perpendicular to the sample surface and scattered ions were detected at a backscattering angle of 160°. In HFS experiments, the incident ion beam probed the sample at a grazing angle of 15°, while the detector counted hydrogen ions that were forward-scattered after

collisions with the probing He^{++} at an angle of 15^{o} with respect to the surface. A thin absorber foil was placed over the detector to filter out the He^{++} ions that were also forward-scattered. The hydrogen concentrations were determined by comparing the hydrogen ion counts from samples under investigation with those obtained from reference samples. A hydrogen-implanted silicon sample and a sample of muscovite with known hydrogen concentrations were used as references. To account for surface hydrogen due to residual moisture or hydrocarbon adsorption, a silicon control sample was analyzed together with the actual sample, and the signal from the control sample was subtracted from that from the actual sample. The estimated absolute experimental uncertainties of the atomic fractions determined by RBS/HFS are ± 1 at% for Hf, ± 3 at% for O, ± 4 at% for C, and ± 2 at% for H.

Imaging of the film surfaces was performed using a JEOL JSM-6700F field-emission scanning electron microscope equipped with an EDAX Genesis XM system for EDS microanalysis. Gold coating of the SEM samples was not needed, because the samples did not charge significantly under the electron beam. In contrast, reference samples of pure HfO_2 showed significant charging effects. This observation suggests that carbon-rich hafnia films have relatively high electrical conductivity. However, in the present study the conductivity was not measured.

Cross-ections of the films were imaged using a Tecnai F20 field-emission TEM equipped with an XT-type objective pole-piece, and operating at an acceleration voltage of 200 keV. The TEM also comprises a Fischione High-Angle Annular Dark Field (HAADF) detector for scanning TEM imaging and an Oxford INCA EDS detector. The TEM samples were prepared by standard mechanical polishing using wedge-polishing technique. The final thinning as well as surface cleaning was performed by Ar^{+} ion milling using GATAN PIPS system. A low energy beam (2-3 keV) and low milling angles (3-6 degrees) were used.

XRD was performed using a Philips XRG 3100 powder diffractometer.

The reported values of the optical bandgap for HfO_2 are 5.6-5.9 eV,[5-9] hence pure HfO_2 is expected to be transparent for 308 nm ($h\nu$ = 4 eV) radiation. However, we found that white sintered HfO_2 targets had sufficiently high absorption at 308 nm to allow efficient ablation by the focused laser beam. This finding wast unexpected, given that sub-bandgap absorption in HfO_2 extending to energies as low as 4 eV has been reported and attributed to intrinsic defects of unidentified type.[6,10,11]

PLD synthesis routes to $HfO_{2-x}C_y$

In this section we describe the two investigated routes for the synthesis of $HfO_{2-x}C_y$ films. Based on published studies, the material that was the target of this study incorporates carbon in the free form, i.e., carbon atoms are primarily bonded with other carbon atoms; thus, it was important to establish that this is also the case in the films synthesized by our two approaches.

In the first synthesis approach, we produced PLD targets by preparing a solid mixture of HfO_2 and graphite powders and pressing the mixture into pellets at room temperature. PLD was performed without background gas. Films obtained using such targets showed relatively high levels of contamination by micron-sized particulates. In general, film quality in PLD is directly related to target quality, i.e., its compactness and surface roughness. Thus, we attempted to improve the quality of HfO_2/graphite pellets by using the finest available grade of graphite powder (-325 mesh) and ball-milling the HfO_2/graphite powder mixture before pressing. This procedure indeed resulted in more compact and finely-grained targets; however, we found that these improved targets did not result in significant improvements of the film morphology. Whereas target modification did not result in better film morphology, we found that deposition on substrates at elevated temperatures had a very favorable effect. Films deposited at 600 °C showed a dramatic reduction in the density of particulates and craters (Fig. 1). A possible reason for the improved film quality at 600 °C is the reduced adhesion of particulates at a hot surface. The film growth rate was reduced by about a factor of 2 compared with room-temperature deposition. The RBS analysis of these films showed incorporation of carbon in the film bulk (Fig. 2). The XPS spectra (discussed in the Year 1 report) showed that the predominant bonding of carbon is C-C, with a small C-O contribution. No evidence was found for Hf-C bonding.

As the second synthesis route, we used pure HfO_2 sintered pellets as targets and C_2H_2 background. Film deposition was performed at room temperature, with C_2H_2 pressures in the range 0.08–2.7 Pa. The choice of C_2H_2 as the source of carbon was guided by its simple molecular structure and prior reports of efficient production of elemental carbon from C_2H_2 both in plasma and on hot surfaces.[12-14] Post-deposition annealing (PDA) at a relatively low temperature of 600 °C was used to reduce the content of hydrogenated carbon and enhance the sp^2 carbon-carbon bonding.

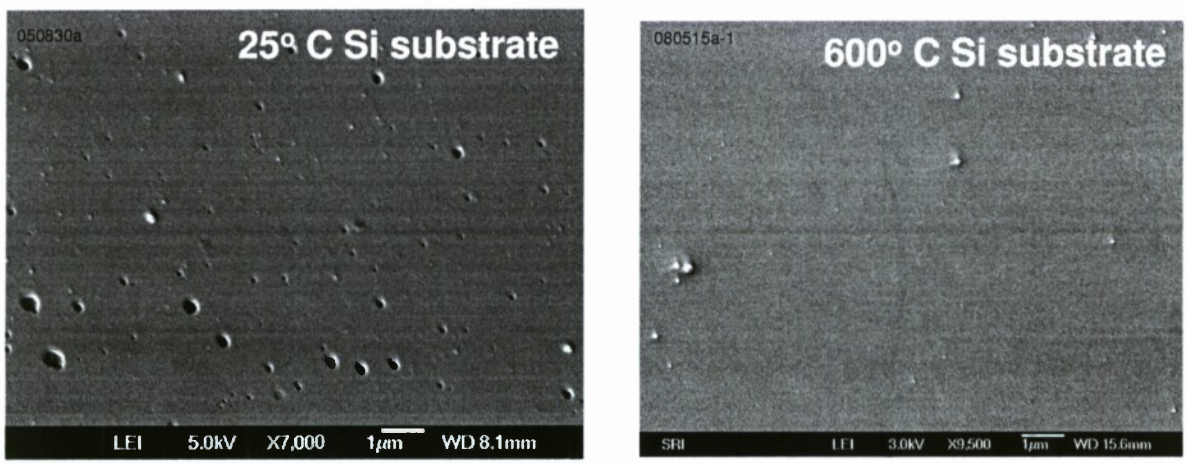

Figure 1. Surface morphology of the films deposited using a HfO_2/graphite target (HfO_2C stoichiometry) with no background gas.

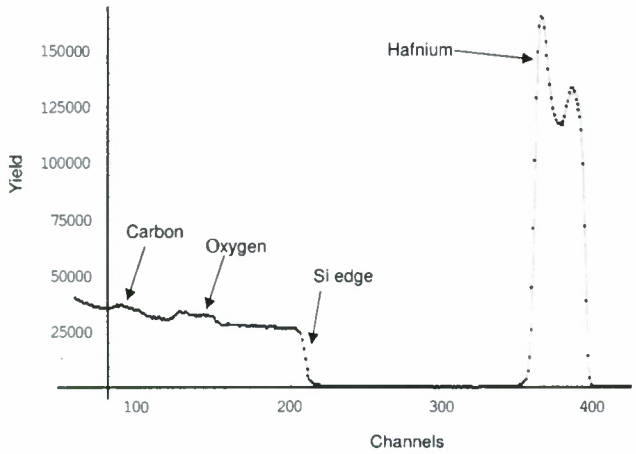

Figure 2. RBS spectrum of a film deposited using a HfO_2/graphite target. (N. Vora, Vanderbilt U.)

It was demonstrated that very high fractions of carbon are incorporated in the films even with low C_2H_2 background pressures, and here we discuss the possible mechanisms for this incorporation. To estimate the total number of carbon atoms available for inclusion in a film by each laser pulse, let us consider a conical volume with its apex at the laser spot on the target and its base of unit area (1 cm^2) at the substrate. Taking a C_2H_2 pressure of 0.2 Pa and the target-substrate distance of 5 cm, at room temperature this volume contains 8.16×10^{13} C_2H_2 molecules, or 1.63×10^{14} C atoms. The RBS analysis found that the number density of C atoms in films deposited at this C_2H_2 pressure was about 1.45×10^{22} cm^{-3}, while the film growth rate estimated from the RBS/TEM film thickness and the number of laser pulses was about 1.2×10^{-9} cm/pulse. Multiplying the last two numbers, it follows that, after each pulse, about 1.7×10^{13} C atoms are deposited per 1 cm^2 of substrate. Therefore, about 11% of the C atoms that were initially contained within the conical volume as C_2H_2 become incorporated in the film after each pulse.

No evidence was found of triply bonded carbon in the films, indicating that trapping of C_2H_2 during film growth is not a significant source of carbon. This implies that C_2H_2 is decomposed by one or more processes during laser ablation, and the products of decomposition (and, possibly, subsequent reactions) are carried toward the substrate by the laser plume. The 308 nm photon energy is insufficient for photodissociation of C_2H_2 in a single-photon process.[15] The carbon molar fraction in the films did not show significant dependence on the laser fluence, indicating that multiphoton photodissociation processes are insignificant as well. The remaining possible routes for C_2H_2 decomposition in the system include (i) thermal decomposition at and near the target surface that is transiently heated by laser pulses, (ii) thermal decomposition in the ablation plume plasma, and (iii) decomposition by impact with energetic particles in the plume.

The route (i) seems insignificant, given that the number of C_2H_2 molecules in the vicinity of a laser-heated spot at the target is a small fraction of the molecules contained within the ablation cone discussed above. In addition, the EDS analysis of the ablated target surface did not indicate the presence of carbon, which would be expected if significant C_2H_2 decomposition at the target surface were taking place. Therefore, decomposition routes (ii) and (iii) are the most plausible sources of carbon in the films. The products of C_2H_2 decomposition (C, C_2, CH, etc.) are likely to react upon reaching the substrate (or film) surface, given their high number density. The products of these reactions may include elemental carbon in various forms and hydrocarbons. How extensive bonding takes place at the surface depends on the surface density and mobility of adatoms. Thus, larger elemental and hydrogenated carbon structures are expected for higher C_2H_2 pressures and higher substrate temperatures.

The films obtained via the HfO_2/C_2H_2 route are of excellent surface quality, with virtually no contamination with particulates. In addition, the film yield is considerably higher than that of

films obtained from HfO_2/graphite targets, and variation of the C_2H_2 pressure allows easy control of the carbon molar fraction in films. Thus, this synthesis route was chosen as the preferred one for further studies. The results of these studies are provided below.

General morphology and surface quality of the films obtained using the HfO_2/C_2H_2 route

Films with thicknesses of up to ~700 nm were deposited on the following substrates: Si, SiO_2 (fused silica), SiC (polished CVD slabs), and highly oriented pyrolytic graphite (HOPG). For Si and HOPG substrates, we verified that even the thickest films were stable and well-adhering even after annealing at 900 °C. This indicates that the films do not have significant strain and can tolerate a significant coefficient of thermal expansion mismatch with these substrates. Figure 3 shows an SEM image of the surface of a sample film. The only features on the otherwise remarkably smooth surface are round particulates, with diameters in the range ~50-300 nm. A weak increasing trend in the surface density of particulates with background C_2H_2 pressure was noticed. This pressure dependence and the relatively small size of particulates suggest that they are formed by nucleation and growth in the vapor phase (which is more effective when there are more collisions between the vapor species and background gas), rather than from solidified liquid droplets expelled from the target (splashing).[16] The EDS/SEM spectrum of the scanned surface (Fig. 3c) shows a strong carbon peak, in addition to the expected Hf and O features, indicating significant incorporation of carbon in the film. The EDS/TEM spot analysis of the spherical particles observed in film cross-sections showed no carbon signal, indicating that these particles consist of pure HfO_2.

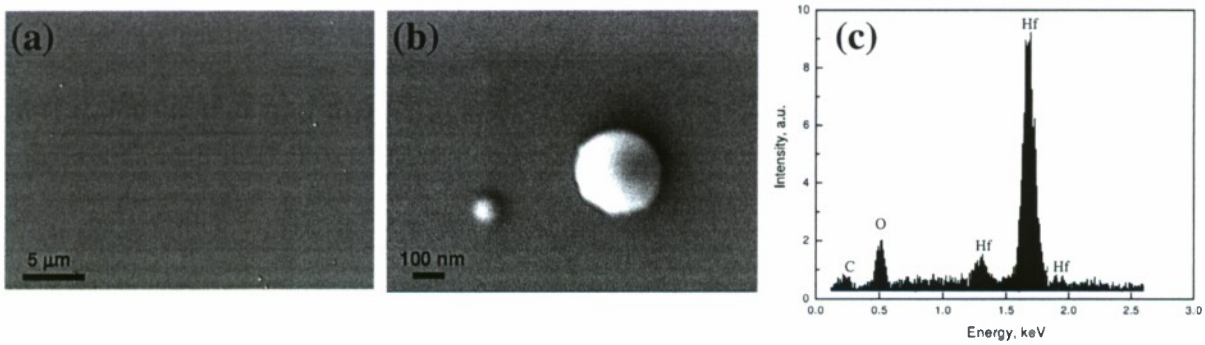

Figure 3. (a) and (b) SEM micrographs of a film grown in 0.2 Pa of C_2H_2, showing nearly spherical sub-micron particles; (c) EDS spectrum of the film surface shown in (a).

Film composition: RBS and HFS analyses

Figure 4 shows a typical RBS spectrum for a 160-nm-thick film obtained using the HfO_2/C_2H_2 route, together with the iteratively adjusted theoretical fit. For each C_2H_2 pressure we performed the RBS analysis on 2–3 samples deposited under nominally identical conditions to assess the sample-to-sample variability of the composition. We found that the composition uncertainty due to this variability was not larger than the experimental uncertainty of the RBS method. Figure 5 provides a summary of the film compositions derived from RBS, for C_2H_2 pressures up to 0.2 Pa. The O/Hf atomic ratio is less than 2 for all samples, although it approaches 2 for the lowest C_2H_2 pressure, which implies that the films contain oxygen-deficient HfO_{2-x}. The result is not surprising, given that oxygen deficiency is commonly observed in films

of HfO_2 and other oxides grown in low-oxygen atmospheres.[10] We note that the interlayer oxide $HfO_{2-x}C_y$ that is the model for this study is also oxygen-deficient. The O/Hf ratio seems to decrease with the C_2H_2 pressure, possibly because C_2H_2 acts as an oxygen scavenger. The C/Hf atomic ratio in the films increases rapidly with the C_2H_2 pressure, and its pressure dependence is consistent with the linear one in the range covered in this work (Fig. 5). We also deposited stable films at a few higher C_2H_2 pressures, up to 2.7 Pa. For these films, we found that the approximately linear dependence between the C/Hf atomic ratio and C_2H_2 pressure shown in Fig. 5 still holds; however, these films were found to be increasingly oxygen-rich. A possible source of this extra oxygen are organic impurities that are present in the C_2H_2 gas. At any rate, films with C/Hf ratios higher than 2 were of no particular interest for this project.

Given that the source of carbon used in this study is a hydrocarbon, the presence of hydrogen in the films was anticipated, and the HFS measurements confirmed it. Figure 6 shows HFS spectra of a film before and after annealing at 600 °C. The atomic concentration of H decreased from about 5% to 1.4% after annealing (Table 1 provides stoichiometry of these samples). Most of the hydrogen is probably present within various forms of hydrogenated carbon, as will be elaborated in the section below that discusses Raman spectroscopy studies.

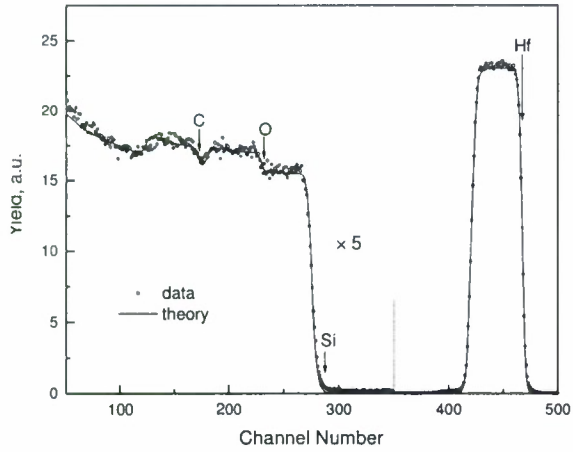

Figure 4. RBS spectrum of a film grown on Si in 0.6 Pa of C_2H_2.

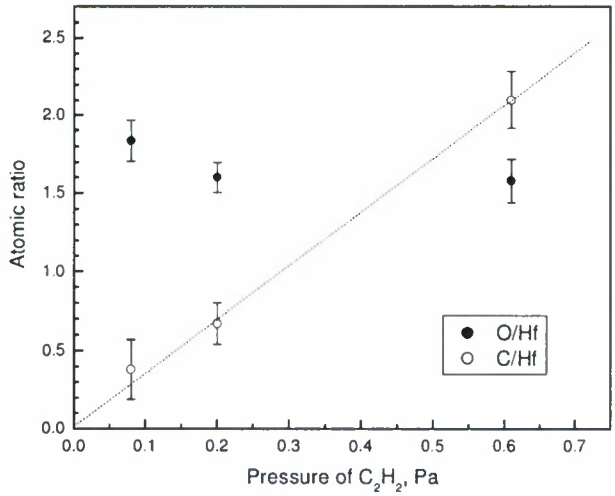

Figure 5. The O/Hf and C/Hf atomic ratios obtained by RBS as functions of the C_2H_2 pressure used during PLD. The error bars represent the RBS experimental uncertainty. The dashed line is guide to the eye.

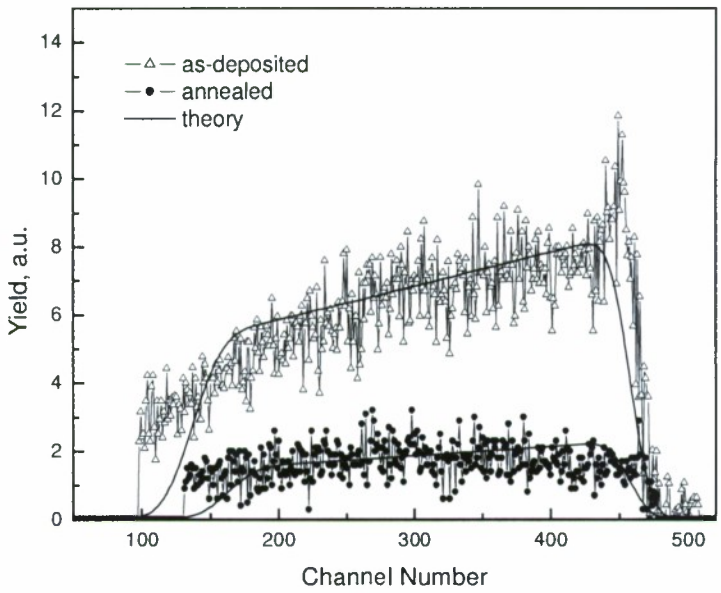

Figure 6. HFS spectra of a film grown in 0.2 Pa of C_2H_2 (upper curve) and of the same film after annealing at 600 °C (lower curve).

Chemical bonding in the films: XPS analysis

Figure 7 shows representative high-resolution XPS spectra in the Hf 4*f*, C 1*s*, and O 1*s* regions for a film grown in 0.2 Pa of C_2H_2 and the same film after PDA in vacuo at 600 °C. A summary of the chemical states identified in these spectra is provided in Table 1. The analysis indicates that Hf is bonded predominantly to O, whereas the principal peak of C is consistent with both carbon- and hydrogen-bonded carbon. The principal state of oxygen is consistent with HfO_2 bonding. The position of the main Hf 4*f* doublet observed in our XPS spectra is somewhat shifted to lower energies compared with the values that are most commonly reported for fully oxidized HfO_2, which indicates that the oxide is oxygen-deficient HfO_{2-x},[17] consistent with the RBS result.

The minor chemical states detected in the film suggest the presence of organic impurities and, possibly, Hf carbide and oxycarbide (Table 1). A probable source of the organics is surface contamination that occurred after deposition. Organics may also be present in the bulk (the estimated probe depth of XPS at a 75° TOA is up to 10 nm), introduced by impurities (such as acetone) that are present in C_2H_2, or produced in reactions of the products of C_2H_2 decomposition with oxygen species ablated from the target. Signatures of carbon-carbon triple bonding that would be indicative of residual C_2H_2 trapped in the film were not observed. The main C 1*s* peak may have a significant contribution from surface contamination by hydrocarbons, as discussed below.

After annealing, the contributions of organic-bonded O and oxygen-bonded C decrease significantly, while the Hf 4*f* spectrum does not show indications of any states other than HfO_{2-x}. The result suggests that annealing removes a significant fraction of the organic constituents, probably via thermal decomposition and subsequent effusion or re-bonding of decomposition products. As noted above, Hf oxide is oxygen-deficient, implying that Hf dangling bonds are present; therefore, oxygen atoms produced by decomposition of organics are likely to bond with Hf. Likewise, it is possible that the carbon atoms and hydrocarbon radicals released from organics subsequently bond into larger hydrocarbon or elemental carbon structures.

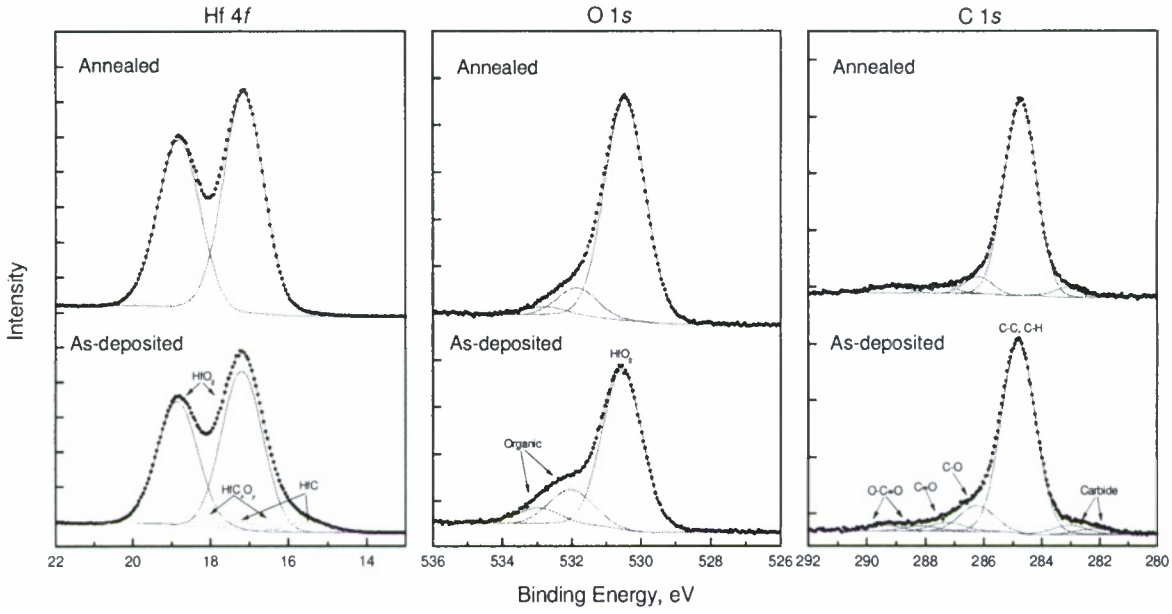

Figure 7. High-resolution XPS spectra of a film grown in 0.2 Pa of C_2H_2 (lower curves) and of the same film after annealing at 600 °C (upper curves). Symbols represent experimental data, red curves represent cumulative multi-peak fit, and curves in other colors represent individual (Gaussian-like) peaks in the fit.

Table 1. Summary of the XPS and RBS/HFS data for a film grown in 0.2 Pa of C_2H_2 and for the same film after annealing at 600 °C.

		As-deposited	**Annealed**
Method	Chemical state	% of total C, O, or Hf	% of total C, O, or Hf
XPS **C** 1*s*	C-C, C-H	75	85
	Carbide	6	4
	C-O	11	6
	C=O	4	3
	O-C=O	5	3
XPS **Hf** 4*f*	HfO_2 or HfO_{2-x}	86	100
	HfC_xO_y (oxycarbide)	8	0
	HfC	6	0
XPS **O** 1*s*	HfO_2	75	85
	Organic	25	15
Stoichiometry from XPS, total		$HfO_{1.99}C_{2.55}$	$HfO_2C_{1.86}$
Stoichiometry from XPS, corrected [a]		$HfO_{1.73}C_{2.22}$	$HfO_{1.7}C_{1.58}$
Stoichiometry from RBS and HFS		$HfO_{1.6}C_{0.67}H_{0.15}$	$HfO_{1.75}C_{0.7}H_{0.05}$

[a] See text.

Table 1 provides stoichiometries, as derived from RBS/HFS, for the films whose XPS spectra are shown in Fig. 7, together with the stoichiometries that were calculated from XPS peak signals in two ways. The "stoichiometry from XPS, total" was calculated using total atomic percentages of Hf, O, and C derived from XPS peak intensities. The "stoichiometry from XPS, corrected" takes into account only the fractions of the three elements that are derived from the dominant XPS peaks, i.e., the fractions of Hf and O that are bonded as HfO_{2-x} and the fraction of C that is bonded as C-C or C-H. The "total" XPS stoichiometry has an O/Hf atomic ratio near 2, and a very high percentage of C. The "corrected" XPS stoichiometry has an O/Hf ratio that is very close to the one derived from RBS; however, the corrected carbon fraction is still considerably higher than that derived from RBS. This result is interpreted as follows. XPS signals are always affected by surface contamination; thus the higher oxygen content found by XPS is partly due to organic impurities (and, possibly, water) that are mostly concentrated in the surface region, which distorts the O/Hf ratio in XPS while not contributing significantly to the RBS data. Thus, by eliminating the contribution of organic chemical states in O 1*s* and Hf 4*f* from the stoichiometry calculation, the correct O/Hf ratio is obtained. Hydrocarbon contaminants are also concentrated in the surface region. However, their contribution to the C-C, C-H peak in XPS is impossible to decouple from the C-C, C-H signal due to elemental carbon and hydrocarbons in the bulk, thus the overestimate of C atomic fraction remains in the corrected XPS stoichiometry.

Film microstructures: TEM and XRD

Figure 8 shows a bright-field TEM (BFTEM) image of the cross section of a 680 nm thick as-deposited film as well as a high-resolution TEM (HRTEM) image of the region adjacent to the Si substrate with the corresponding selected-area electron diffraction (SAED) pattern. The structure of the film is clearly disordered, with neither HfO_2 nor carbon forming nanocrystallites and a SAED pattern that shows only diffuse rings due to short-range ordering. TEM of other as-deposited samples showed very similar microstructures. The EDS/TEM analysis performed for a number of different spots in a film cross section always showed peaks of all three main constituent elements (Hf, O, and C), with relative peak intensities that did not vary significantly

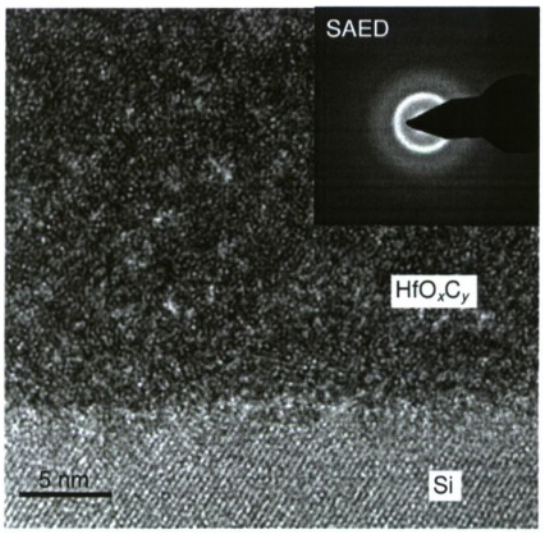

Figure 8. HRTEM image of an HfO_xC_y film grown in 0.2 Pa of C_2H_2. Inset: SAED pattern for the film.

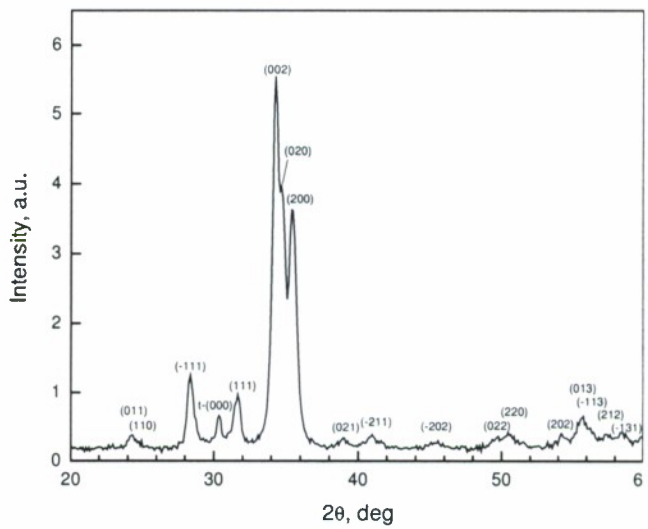

Figure 9. XRD pattern of a film grown in 0.08 Pa of C_2H_2 and annealed at 600 °C in vacuo.

from spot to spot. Given that the estimated resolution of the EDS/TEM spot analysis is ~5 nm, this indicates that carbon and HfO_2 are mixed on a very short length scale.

The microstructures of annealed films showed strong dependence on the carbon molar fraction. For the films grown in 0.2 and 0.6 Pa of C_2H_2, after PDA the microstructures were virtually unchanged, with featureless XRD patterns and no indications of microcrystallinity or phase separation between HfO_2 and carbon in TEM images. However, PDA at 600 °C of films grown in 0.08 Pa of C_2H_2 caused crystallization of HfO_2. The XRD pattern (Fig. 9) shows that HfO_2 crystallized in the expected monoclinic phase. The intensities of peaks (002), (020) and (200) are several times higher than is expected for randomly oriented crystallites, indicating that HfO_2 crystallites form with these orientations as preferred ones. The origin of this preferred orientation is currently not understood. The average size of crystallites, determined from XRD peak broadening, was found to be about 16 nm.

One of the XRD peaks found is not consistent with the monoclinic phase, but it can be assigned to the (000) plane of the tetragonal phase (Fig. 9). Other tetragonal phase peaks were not observed, hence it cannot be asserted that the tetragonal phase is indeed present. It is possible that (000) is the preferred orientation for growth of tetragonal crystallites, which would explain the enhanced intensity of the (000) diffraction. At any rate, while the stable phase of bulk HfO_2 at room temperature is the monoclinic one, the presence of minor tetragonal phase is possible when the crystalline HfO_2 is formed by annealing from amorphous HfO_2. In fact, published work indicates that crystallization of HfO_2 into tetragonal phase seems to be preferred when the amorphous precursor has a large surface area[18] and when long-range structural order is inhibited by geometrical constraints[19] or by mixing with other oxides.[20,21]

Films of pure HfO_2 grown by PLD at room temperature are typically amorphous,[22] and it is thus not surprising that the as-deposited films studied here are amorphous as well. However, in pure HfO_2 films the development of microcrystallinity upon PDA is expected for annealing temperatures as low as 400-450 °C.[23-25] As the contrasting annealing behavior of films with different C/Hf ratios shows, high carbon content has the effect of stabilization of the amorphous structure of HfO_2. The issue of the inhibition of crystallinity by carbon addition is discussed in more detail below.

Forms of carbon in the films: Raman spectroscopy

Raman spectroscopy provided key insights into the form of carbon present in the films. The Raman spectra of disordered carbons that contain sp^2 bonds show two characteristic features: the G band around 1560 cm^{-1}, which is due to the stretching vibrations of pairs of sp^2 C atoms in both rings and chains (E_{2g} mode);[26,27] and the D band around 1360 cm^{-1}, which is forbidden in perfect graphite and appears in the presence of disorder due to double resonant Raman scattering.[28]

The Raman spectra for as-deposited and annealed films grown in 0.08 Pa of C_2H_2 are shown in Fig. 10. The spectrum for the as-deposited film shows only a weak, very broad band in the region 1000-1600 cm^{-1}, which cannot be assigned to any form of carbon, and is possibly a second-order spectral feature due to phonon scattering of the amorphous HfO_2 film.[29] The strong band at 960 cm^{-1} is due to optical phonon scattering of the Si substrate.[30] For the annealed sample, it was found that the spectra were strongly dependent on the position on the sample surface—a behavior not observed for samples with higher carbon contents. For all surface spots probed, the spectra show a baseline that increases with the Raman shift. This is the

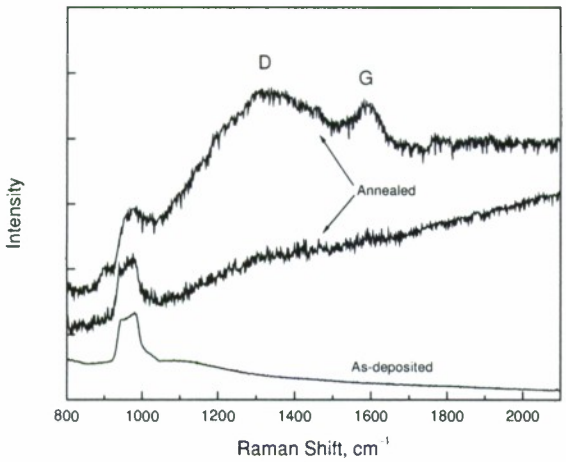

Figure 10. Raman spectra of a film grown in 0.08 Pa of C_2H_2 (bottom curve) and of the same film after annealing at 600 °C, probed at two different surface locations (upper two curves).

photoluminescence (PL) background that is a well-known signature of various forms of amorphous hydrogenated carbon (a-C:H).[31,32] The PL background is expected to increase with the H content, due to the hydrogen saturation of nonradiative recombination centers,[32] and for carbons with H atomic contents over ~45% the background usually overshadows the Raman features of a-C:H.[26,32,33] These carbons are usually referred to as polymer-like a-C:H (PLCH) and are characterized by a high fraction of sp^3 bonds, which are mostly H-terminated.[31] Notwithstanding the similarity between the Raman spectra of PLCH and that of the annealed carbon-rich hafnia film in Fig. 10, the two carbon systems are obviously very different; the film has an H/C atomic ratio less than 0.1, which is much lower than the ratios (~1) characteristic for PLCH. Unlike hydrogenated carbon in PLCH, carbon in here studied films is trapped within a HfO_{2-x} matrix, which may inhibit formation of sp^2-bonded carbon domains and cause the sp^2 Raman features to be much weaker than what would be expected for pure hydrogenated carbon.

Upon annealing of hydrogenated carbons at 600 °C, significant effusion of bonded hydrogen is expected, leading to loss of hydrogen from samples.[33,34] The HFS measurements that were presented above confirmed significant hydrogen loss, while no significant carbon loss on PDA in vacuo was detected. Given that as-deposited films contain more hydrogen than annealed ones, it is not obvious why the film deposited at 0.08 Pa of C_2H_2 shows the PL background characteristic for a-C:H only after PDA. A probable reason for this is that the as-deposited film, given its low overall carbon concentration, actually contains mostly small hydrocarbon molecules and, possibly, small clusters of elemental carbon. In contrast to extended structures of a-C:H, these smaller species of carbon do not produce the PL background. Annealing leads to a reduction in hydrogen content and reordering of carbon into extended networks of a-C:H, characterized by the PL. This is probably accompanied by enhanced ordering of the existing sp^2 phase and the conversion of some sp^3 sites into sp^2 sites.[34,35]

For some probed spots, the Raman spectra of the annealed film grown in 0.08 Pa of C_2H_2 show the D and G peaks in addition to the PL background (Fig. 10), indicating that at these locations the H content is lower and/or the fraction of sp^2 carbon is higher than in the spots that do not show these peaks. The non-uniformity in the spatial distribution of hydrogenated carbon observed in the annealed film is probably related to HfO_2 crystallization, discussed earlier. The formation of HfO_2 crystallites is expected to augment any inherent non-uniformity of the carbon distribution that had been present in the film before crystallization took place. The regions with lower initial carbon concentration crystallize earlier and form larger crystallites, which drives the migration of carbon to neighboring spatial regions. Therefore, it is plausible that crystallization of HfO_2 leads to coalescence of carbon domains, and in these enlarged domains the formation of

extended sp^2 carbon chains and rings is likely at 600 °C. Surface spots that contain such carbon will thus have enhanced D and G peaks.

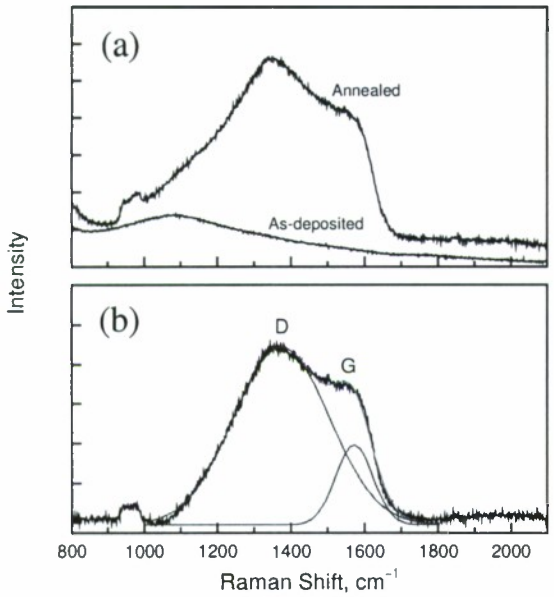

Figure 11. Raman spectra of a film grown in 0.2 Pa of C_2H_2: (a) spectra measured before and after annealing at 600 °C; (b) background-subtracted spectrum for the annealed film (black) is shown together with the cumulative two-peak Gaussian fit (red) and individual Gaussians (blue).

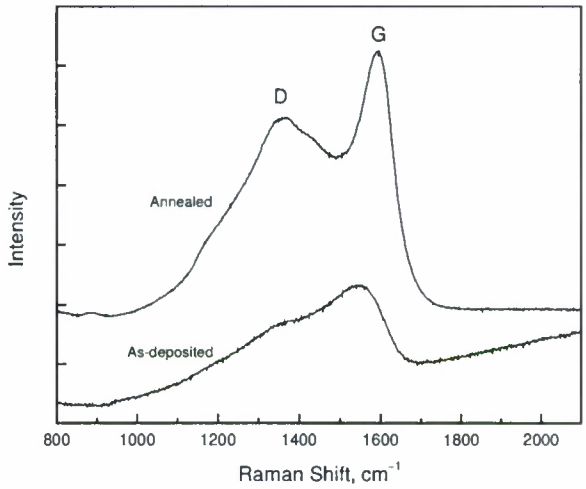

Figure 12. Raman spectra of a film grown in 0.6 Pa of C_2H_2 (lower curve) and of the same film after annealing at 600 °C (upper curve).

The Raman spectra for the as-deposited and annealed films deposited in 0.2 Pa of C_2H_2 are shown in Fig. 11. The as-deposited sample spectrum again does not show any carbon features. However, the annealed sample spectrum shows much stronger sp^2 carbon features than those observed in the sample deposited at the lower C_2H_2 pressure, and the PL background contribution is negligible. This spectrum is similar to those of a-C:H with a hydrogen content less than 20%, usually referred to as the graphite-like a-C:H (GLCH).[31] Given that the RBS/HFS data indicate that not more than 7% of carbon in this annealed sample is hydrogenated (Table 1), carbon in this film may also be categorized as nano-graphitic.

For films grown in 0.6 Pa of C_2H_2, the signatures of graphitic carbon are present even before annealing (Fig. 12). Based on a qualitative comparison of the sizes of sp^2 carbon peaks with that of the PL background, the spectrum is very similar to those of a-C:H with an intermediate (20-40%) H content and a lower sp^3 content than that of PLCHs, in the literature referred to as the diamond-like a-C:H (DLCH).[31] After PDA, the sample shows well-defined G and D peaks, consistent with the behavior of GLCH or nano-graphitic carbons.

One of the parameters used to characterize the carbon bonding in various forms of carbon is the full width at half maximum of the G peak ($FWHM_G$), which increases as disorder increases.[31,33,36] By fitting the Raman spectra with two Gaussians (Fig. 11), we extracted $FWHM_G$, and found that it decreases with annealing for films grown in 0.6 Pa of C_2H_2. This

indicates increased ordering of the sp^2 regions that accompanies the effusion of hydrogen species. A weak decreasing trend in $FWHM_G$ with increasing carbon content in the annealed films is also observed. The increase of the sp^2 ordering with C content in the annealed films possibly results from better initial ordering in as-deposited films with higher C concentration, given that higher surface density of C adatoms implies higher probability of formation of extended sp^2 chains and rings.

The observed effects of PDA can be explained as follows. Thermal effusion measurements of a-C:H films have shown that the peak of effusion occurs at 600 °C, and the main effusion species is H_2, while minor species include H, CH_4, C_2H_4 , CH_3, and other hydrocarbons.[34] It is likely that elemental hydrogen is the dominant effusion species in our films as well, given that annealing significantly reduces the H content, while the C content is not affected significantly. Hydrogen loss is accompanied by the conversion of sp^3 sites into sp^2 sites, as has been reported for annealed a-C:H.[34,35,37] In addition, ordering in the existing sp^2 regions is improved and it is likely that some neighboring sp^2 regions coalesce. This structural evolution of carbon is reflected in the enhanced sp^2 vibrational modes and, in particular, sharpening and increase of the Raman D peak.

Annealing of the $HfO_{2-x}C_y$ films in O_2

One of the important questions in the present study, central to understanding the role of $HfO_{2-x}C_y$ interlayers in controlling the oxidation kinetics of HfC, was the question of stability of the $HfO_{2-x}C_y$ system in oxidizing environments at elevated temperatures, i.e., to what extent is the structure capable of retaining carbon. This question is also important for assessing the applicability of the $HfO_{2-x}C_y$ system for protective coatings. We found that in oxidizing environments $HfO_{2-x}C_y$ films do not retain carbon well, even at relatively low temperatures. Figure 13 shows EDS spectra of an as-deposited film, and of the same film after annealing at 550 °C in Ar and in O_2 (pressure 400 Pa). Whereas annealing in inert atmosphere does not appreciably change the carbon relative signal, after annealing in O_2 most of carbon is lost. SEM images of surfaces of films annealed in O_2 show fissures (Fig. 14a) that become more pronounced for films with higher initial carbon content (Fig. 14b). This indicates that the fissures are produced by the gaseous products of carbon oxidation (CO and CO_2), which are generated in large enough quantities to disrupt the film surface upon volatilization.

As the next step, we investigated whether carbon lost by oxidation from a $HfO_{2-x}C_y$ film

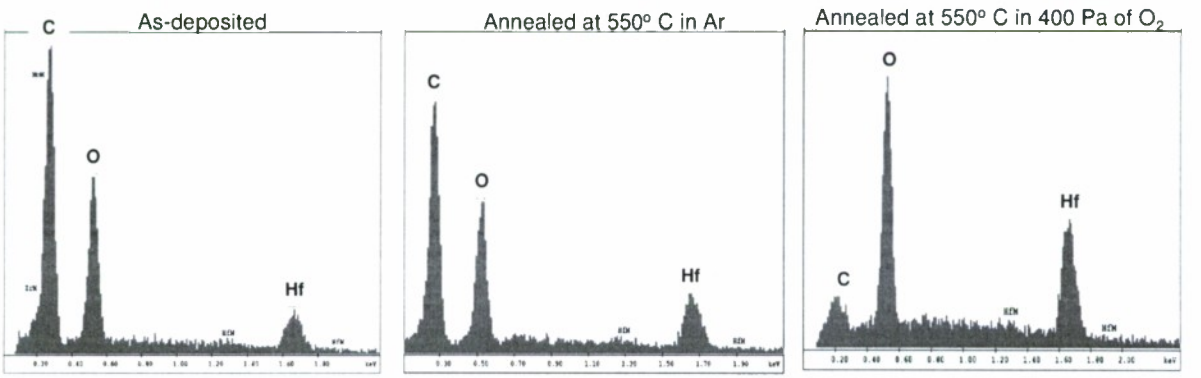

Figure 13. EDS spectra of the surfaces of films grown in 1.4 Pa of C_2H_2 before and after annealing for 30 min at 550 °C in Ar and O_2.

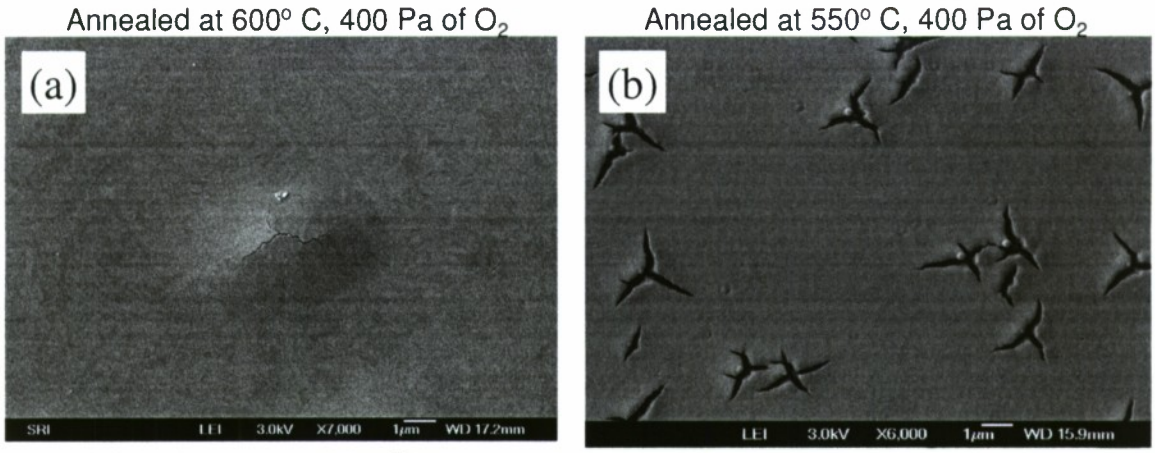

Figure 14. SEM images of the film surfaces after annealing for 30 min in 400 Pa of O_2. (a) Film grown in 1.4 Pa of C_2H_2; (b) Film grown in 2.7 Pa of C_2H_2.

can be partly re-supplied by diffusion from an underlying carbon-bearing substrate. The most important substrates from the point of view of applications are carbon-carbon composites; however, these materials do not have sufficiently high surface quality to allow deposition of high-quality thin films and sensitive post-deposition analysis of the film microstructure and composition. Thus, we chose the form of carbon with the highest surface quality—HOPG. The $HfO_{2-x}C_y$ films on HOPG were annealed in 67 Pa of O_2 at a temperature of 600 °C for 30 min, and their cross-sections were subsequently analyzed by TEM and EDS/TEM. A TEM image of such a cross-section is shown in Fig. 15a. A straight line in the image indicates the region in which the EDS line scan, shown in Fig. 15b, was performed. The image shows relatively large crystallites in the film, which indicates that most of the carbon was removed from the film by oxidation, which enabled crystallization of HfO_2. The EDS scan shows very low carbon signal in the film, confirming this interpretation. The HfO_2 crystallites formed even in the close proximity of HOPG, and there are no indications of either carbon retention or carbon replacement near the film/HOPG interface (the gradual signal profiles near the interface in Fig. 15b are probably due to the limited lateral resolution of the EDS probe of ~ 5nm).

Given the rapid loss of carbon from thin $HfO_{2-x}C_y$ films in oxidizing environments, we

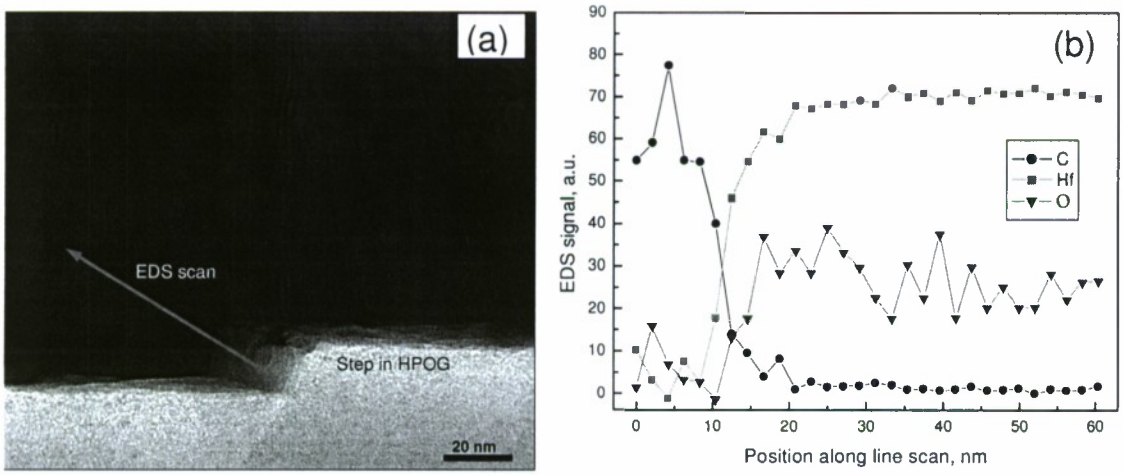

Figure 15. (a) TEM image of the cross-section of a $HfO_{2-x}C_y$ film on HOPG substrate. The film was grown in 0.5 Pa of C_2H_2 (C/Hf ratio ~1.6) and annealed at 600 °C in 67 Pa of O_2 for 30 min. (b) Variation of EDS atomic signals along the line indicated by the arrow in (a).

can draw the following conclusions. Thin (<1 μm) $HfO_{2-x}C_y$ films *per se* are not suitable as protective coatings in oxidizing environments. It is possible that much thicker $HfO_{2-x}C_y$ coatings or multi-layer coatings that incorporate $HfO_{2-x}C_y$ would show some protective properties, however the production of such coatings was beyond the scope of this project. Going back to the role of $HfO_{2-x}C_y$ interlayer oxide in oxidation of HfC, our results suggest that the top portion of this interlayer becomes converted very quickly into low-carbon, microcrystalline, and porous HfO_2, and the consistency of the interlayer during oxidation is maintained only via conversion of HfC into $HfO_{2-x}C_y$ at the other interface in the system. When considering protective properties of $HfO_{2-x}C_y$ in the $HfC/HfO_{2-x}C_y/HfO_2$ system, the interlayer thus must be viewed as a dynamic entity. The protective properties of the $HfO_{2-x}C_y$ interlayer seem to stem solely from the relatively slow diffusion of oxygen (compared to that of the outer HfO_2 layer), not from the oxidation resistance of the interlayer *per se*.

The amorphous/microcrystalline transitions in $HfO_{2-x}C_y$ layers

An intriguing feature of the $HfC/HfO_{2-x}C_y/HfO_2$ system is the strikingly sharp interface between $HfO_{2-x}C_y$ and HfO_2, and one of our goals was to reveal the reasons for the formation of such an abrupt boundary. To achieve this, we deposited relatively thick $HfO_{2-x}C_y$ films with several different carbon fractions, and subjected them to very slow oxidation such that carbon from the films is gradually removed without disrupting the film surfaces. The cross-sections of oxidized films were then imaged by TEM and carbon depth profiles analyzed by EDS in TEM.

An EDS depth line scan for an as-deposited film grown in ~0.61 Pa of C_2H_2 is shown in Fig. 16a. The point-to-point variation of the EDS carbon signal is probably inherent to the method; however, there seems to be a weak systematic trend of carbon concentration increase towards the film surface. This increase is probably due to the observed drift in the C_2H_2 pressure during PLD from 0.57 to 0.68 Pa. Figure 17 shows a TEM image of the cross section of the same film after PDA in ~0.01 Pa of O_2 at 550 °C for 50 min. An outer layer, comprising about a half of the film thickness, shows markedly different TEM contrast from the bottom half of the film. The HRTEM image in Fig. 17 reveals the presence of nano-crystallites in the upper layer, which are absent in the bottom sub-layer. This observation is supported by SAED patterns, which show spots with higher intensity in the upper layer, while the bottom layer produces again only ring-like features (Fig. 17). The EDS depth line scan (Fig. 16b) shows that annealing has produced a

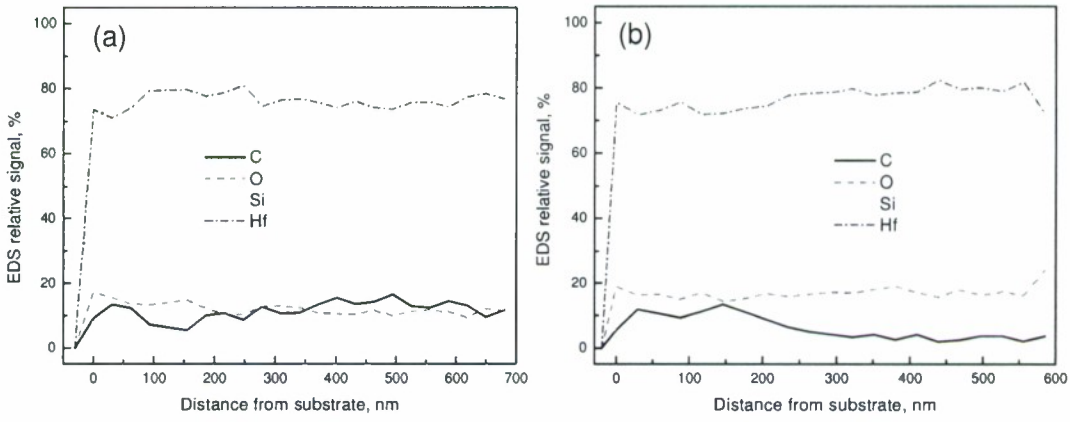

Figure 16. EDS/TEM elemental depth profiles for a film grown in 0.61 Pa of C_2H_2: (a) as-deposited film; (b) film annealed at 550 °C for 50 min in ~0.01 Pa of O_2.

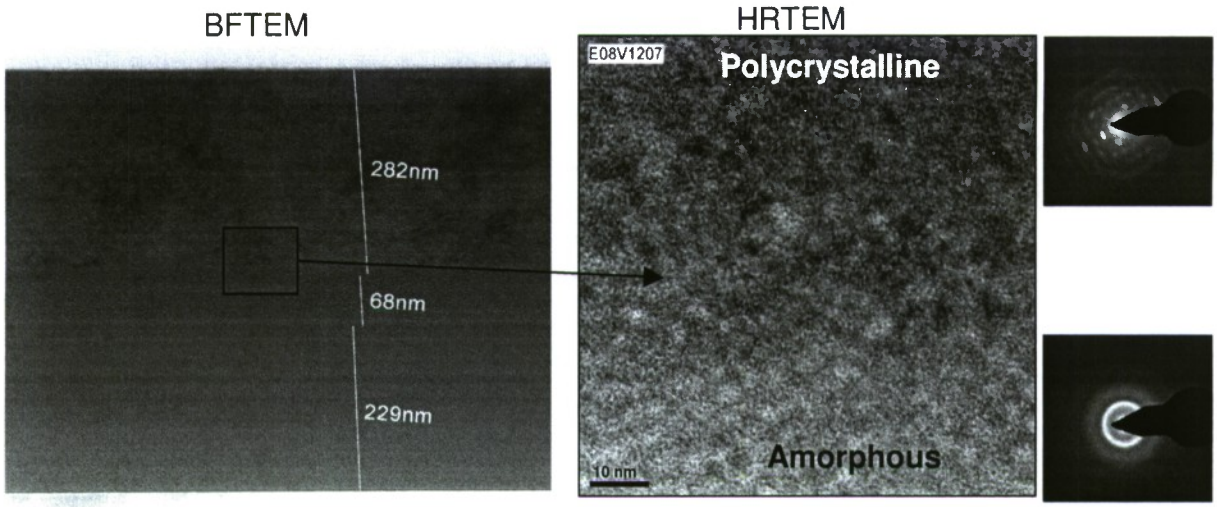

Figure 17. Left: Bright-field TEM image of the cross-section of the annealed film whose EDS depth profile is shown in Fig. 16b. Right: high-resolution TEM image of the region between two sub-layers in the film with SAED patterns for the two sub-layers.

pronounced depth variation of carbon content in the film. The carbon concentration is high and nearly constant in the bottom ~200 nm of the film (corresponding approximately to the amorphous sub-layer), and then decays towards the film surface. A plausible explanation for the microstructure and carbon concentration profile observed in the cross-section of the annealed film is that removal of carbon from the top layer by slow oxidation facilitates crystallization of HfO_2 in this portion of the film. It seems that, once microcrystallites form, oxygen diffusion becomes faster, which further accelerates the loss of carbon; this explains the rather abrupt drop in the carbon concentration between the sub-layers. The sharp boundary that forms between the two sub-layers indicates that there is a well-defined threshold value of carbon concentration above which the material resists crystallization, which is an important conclusion for understanding the occurrence of the analogous boundary between the $HfO_{2-x}C_y$ and HfO_2 layers in oxidized HfC.[2,3,38,39].

The film grown in 0.61 Pa of C_2H_2 was analyzed in the analogous manner after slow oxidation at 900 °C. In this case, no O_2 was added into the system, but it is estimated that ~10^{-3} Pa of O_2 was present due to a small residual leak in the furnace. Oxidation due to this small leak again led to the loss of carbon and crystallization in the top portion of the film, while the bottom portion remained carbon-rich and mostly amorphous (Fig. 18). EDS showed that the carbon concentration drop across the boundary between the two sublayers is in this case very abrupt (Fig. 18), confirming the existence of a threshold carbon concentration for the amorphous-to-crystalline transition. We emphasize that the carbon-rich (carbon molar fraction of ~0.4) sub-layer remained mostly amorphous even at 900 °C, while pure HfO_2 is typically reported to crystallize at temperatures below 500 °C. A contrasting behavior was observed in a film with lower initial carbon content, grown in 0.2 Pa of C_2H_2, which was treated at 900 °C simultaneously with the above discussed sample grown in 0.61 Pa of C_2H_2. This film shows a high level of crystallinity throughout its cross-section; starting from a lower initial carbon content, oxidation reduced the carbon fraction below the threshold value for crystallization in the entire film (Fig. 19).

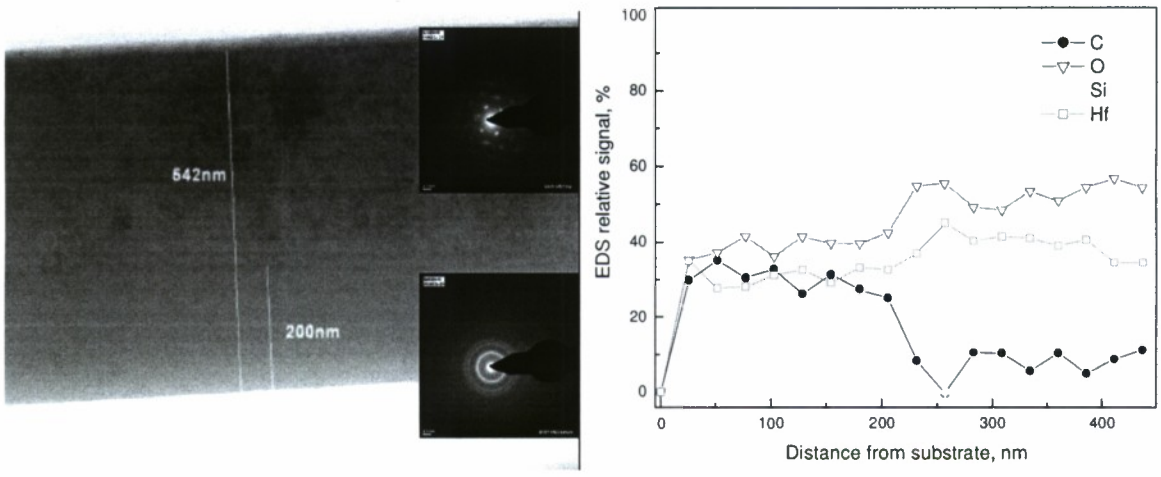

Figure 18. Left: TEM image of the cross-section of a film grown in 0.61 Pa of C_2H_2 and annealed at 900 °C in ~10^{-3} Pa of O_2 (see text), with SAED patterns for the two sub-layers. Right: EDS elemental depth profiles for this film.

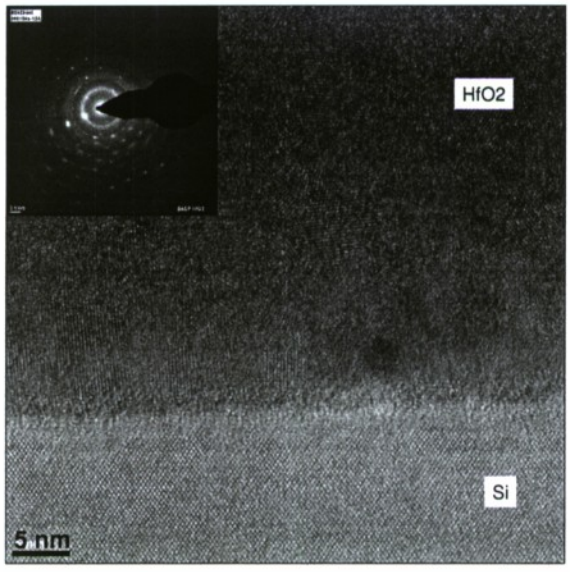

Figure 19. TEM image of the cross-section of a film grown in 0.2 Pa of C_2H_2 and annealed at 900 °C in ~10^{-3} Pa of O_2. Part of the film near substrate is shown, together with the corresponding SAED pattern.

Oxygen diffusion in $HfO_{2-x}C_y$ films

To investigate oxygen diffusivity in the films, we performed brief anneals in isotopically-enriched O_2 at an elevated temperature (550 °C), and analyzed the films by SIMS to trace the ^{18}O depth profiles. Figure 20 shows SIMS elemental depth profiles for the amorphous film whose EDS profiles were shown in Fig. 16a. The ^{18}O concentration drops to the natural abundance level of 0.2% within the top ~150 nm from the film surface. In the top portion of the film, the comparison of the ^{18}O and ^{16}O profiles shows that significant atom exchange between the diffusing ^{18}O atoms and lattice ^{16}O atoms occurred. This is not surprising, given that the

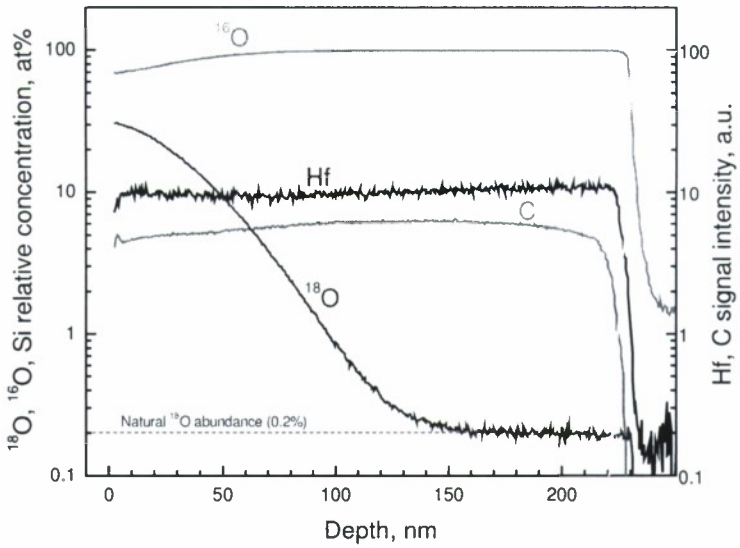

Figure 20. SIMS elemental depth profiles for an amorphous film grown in 0.61 Pa of C_2H_2 after annealing in ^{18}O-enriched O_2 at 550 °C.

published work on oxygen diffusion in pure HfO_2 indicates that the lattice exchange is the dominant oxygen diffusion mechanism in this material.[40, 41] In this process, the O atoms within the oxide lattice framework are substituted by oxygen atoms (including ^{18}O) from the gas phase. The total oxygen content of the oxide remains constant during exchange, which is different from the case of interstitial incorporation and diffusion, where the oxygen content increases.

Figure 21 shows the SIMS profiles for the two-layer (amorphous-microcrystalline) film from Fig. 16b. The ^{18}O concentration is considerably higher than the natural abundance level in the entire, ~250-nm-thick upper sub-layer with microcrystalline (carbon-depleted) structure. This indicates that ^{18}O supplied from the gas phase has diffused throughout the top sub-layer, which, upon comparing with Fig. 20, implies that the oxygen diffusivity is considerably faster than in the amorphous, carbon rich film. Further confirmation of this effect of microstructure on the oxygen diffusivity is observed in the two-layered film itself: The ^{18}O signal drops abruptly to the 0.2% natural abundance level when crossing from the microcrystalline sub-layer into the bottom (amorphous and carbon-rich) sub-layer (Fig. 21). These results support the diffusion modeling results of Bargeron et al.[1-3] and one of the main hypotheses that motivated this project: that the carbon-rich amorphous $HfO_{2-x}C_y$ layer acts as a better oxygen diffusion barrier then carbon-depleted microcrystalline HfO_2.

Another interesting observation is that the ^{18}O-^{16}O exchange is weaker in the carbon-depleted layer (Fig. 21) than in the carbon-rich film (Fig. 20). To interpret this observation, it is important to note that published calculations[42] of oxygen incorporation and diffusion energies in HfO_2 have suggested that oxygen incorporates and diffuses in the form of atomic ions. The extent of the atom exchange in the oxide thus depends on the availability of atomic oxygen at the surface. It is expected that O_2 molecules adsorb on oxide surfaces and dissociate primarily at O-vacancy defect sites.[43] The amount of available O atoms depends on the rate of dissociation of O_2 at the surface, hence it depends on the density of O vacancies at the surface. Therefore, a possible reason for the higher exchange fraction in the amorphous carbon-rich film is a higher density of O vacancy sites at the film surface, or a higher density of some other defect sites that may favor O_2 dissociation. Here "defect" means any deviation from perfect HfO_2 structure, and may include carbon sites. As discussed above, $HfO_{2-x}C_y$ films are oxygen deficient, thus a high

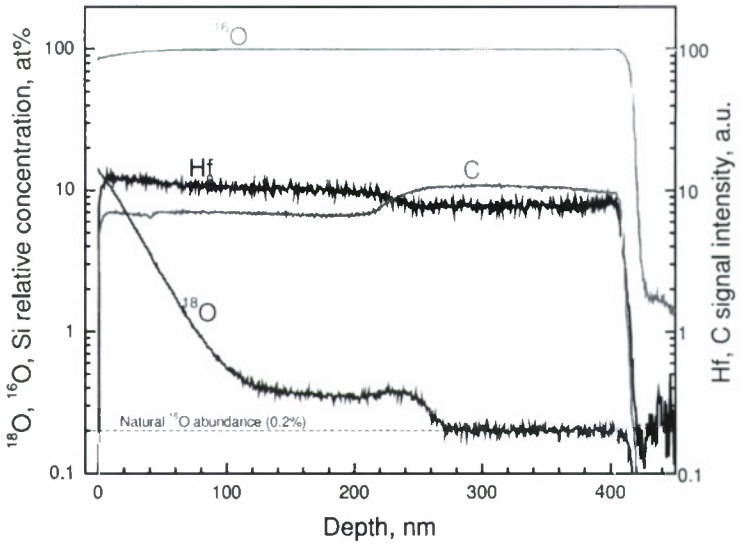

Figure 21. SIMS elemental depth profiles for the two-layered film from Fig. 17 after annealing in ^{18}O-enriched O_2 at 550 °C.

concentration of O vacancy sites is indeed expected. Moreover, annealing in the presence of oxygen, which produced the partly crystallized two-layered film, may have decreased the concentration of oxygen vacancies at the surface, thus leading to a lower rate for O_2 dissociation at the surface of this film. As a result of the higher availability of atomic oxygen at the surface, the amorphous carbon-rich film has higher effective oxygen *permeability* than the microcrystalline carbon-depleted layer, despite the lower oxygen diffusion rate in it. This does not imply that in two-layer systems such as the ones in Figs. 17 and 18 the carbon-rich layer will not present an affective oxygen diffusion barrier, given that the availability of atomic oxygen is determined by the external, carbon-depleted microcrystalline layer.

To estimate the oxygen diffusivity in the amorphous $HfO_{2-x}C_y$ film, the ^{18}O SIMS profile from Fig. 20 was fitted with the well known functional form[42,43]

$$\frac{c(z)-c_0}{c_{gas}-c_0} = \mathrm{erfc}\left(\frac{z}{2\sqrt{Dt}}\right) - \exp\left(hz + h^2 Dt\right)\cdot \mathrm{erfc}\left(\frac{z}{2\sqrt{Dt}} + h\sqrt{Dt}\right), \qquad (1)$$

where $c(z)$ is the depth-dependent ^{18}O concentration, z is depth, c_0 is the background ^{18}O concentration (in this case the natural abundance level), D is the diffusion coefficient, t is time, and $h = \alpha/D$, where α is the surface exchange coefficient that quantifies the oxygen exchange across the gas/solid interface. Figure 22 shows the fitted ^{18}O depth profile. Figure 23 plots the value of D (3×10^{-14} cm^2s^{-1}) extracted from the fit together with the high-temperature values of the oxygen diffusion coefficient in the $HfO_{2-x}C_y$ interlayer oxide reported by Bargeron et al.,[1-3] who obtained these values using a moving-boundary model of HfC oxidation. The value we extract at 550 °C is a factor of ~15 lower than that value obtained when the two high-temperature values reported by Bargeron et al. are fitted with a line on an Arrhenius plot and the line is extrapolated to lower temperatures. In the two-layered film in Fig. 21, the amorphous bottom layer acts as a diffusion barrier, thus back diffusion must be considered as well. This is a more complicated modeling task and it was not performed in this project. We note that, given that the film contains carbon that rather rapidly oxidizes in the presence of O_2, an accurate qualitative analysis of the SIMS profile in Fig. 20 should include coupled reaction (e.g., O + C → CO) and

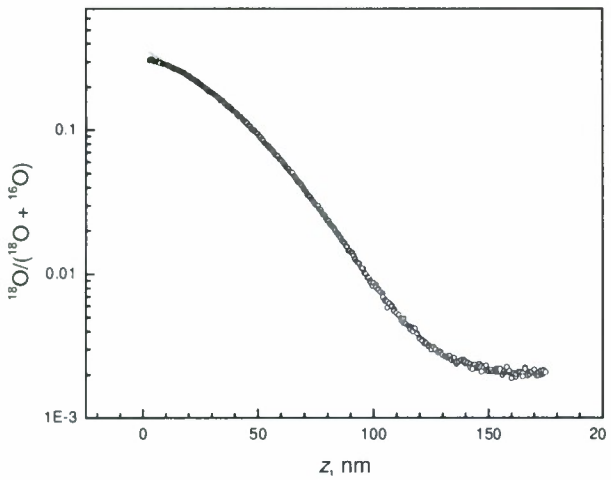

Figure 22. The ^{18}O diffusion profile for amorphous film from Fig. 20 (symbols) fitted with the functional form (1) (line).

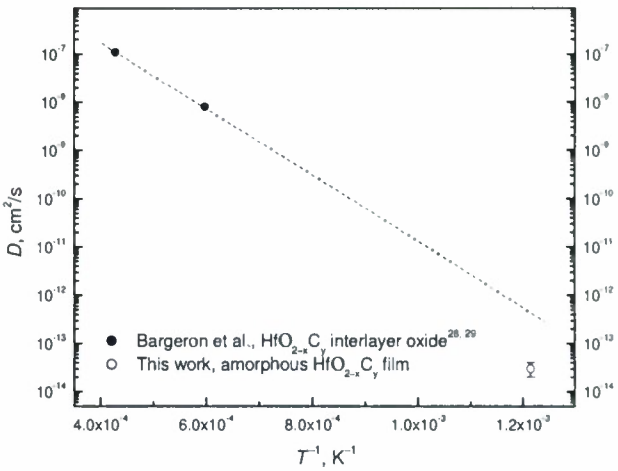

Figure 23. The value for the oxygen diffusion coefficient for amorphous $HfO_{2-x}C_y$ film at 550 °C and literature[1-3] values extracted by modeling HfC oxidation at high temperatures.

diffusion equations; thus the values of D we extracted may have a significant uncertainty. Here we assume that at the relatively low annealing temperature of 550 °C the relative loss of ^{18}O in the reaction with carbon is not very significant, and that consequently the ^{18}O depth profiles are controlled primarily by diffusion. We plan to analyze the measured SIMS profiles by a more sophisticated diffusion-reaction model in the near future. The main qualitative conclusion—that oxygen diffusion is slower in the amorphous, carbon-rich layers, should be robust even in the presence of small ^{18}O reactive losses.

Phosphorescence and thermoluminescence (TL) of HfO_2

This part of the research effort was motivated by the PI's observation of strong and long-lasting phosphorescence of HfO_2 targets irradiated with UV laser beam. Subsequently, the PI also observed phosphorescence in thin PLD films of pure HfO_2. Although the phosphorescence of HfO_2 doped with Ti has been known since 1994,[44] this effect has been largely disregarded in the literature since then. Besides, the phosphorescence of nominally pure HfO_2 is a novel finding and deserved further inquiry. In general, phosphorescence in solids is a result of charge trapping centers that capture photogenerated charge carriers until detrapping occurs by thermal excitation. The issue of charge trapping in HfO_2 is central to the envisioned application of this oxide as a high-dielectric-constant dielectric in downscaled metal-oxide-semiconductor (MOS) devices,[45] thus studies of phosphorescence and TL of HfO_2 can provide information important to the control of the dielectric properties of this material. This study was also pertinent to the main subject of this project; we found that the phosphorescence strongly depends on the microstructure (and possibly stoichiometry as well) of HfO_2 and, as shown above, this microstructure is also key to the properties of carbon-rich hafnia. Moreover, once firmly established, the correlation between the luminescent properties on one side, and microstructure/composition on the other can be used to develop reliable and quick optical diagnostics of the microstructure of components based on HfO_2 following various treatments that they may undergo in high-temperature applications. Most of the study was funded by internal

SRI funds; however parts of the effort with a more direct relevance to this project (i.e., luminescent properties of thin films) were supported by the project's funds.

Background

There have been several studies of the phosphorescence and TL of Ti-doped and nominally pure ZrO_2, a material exceedingly similar to HfO_2, and the origin of these effects has been controversial. It has been suggested that the phosphorescence in ZrO_2 is of intrinsic origin, and related to the asymmetric coordination of the Zr^{4+} ion in monoclinic ZrO_2 by 7 O atoms.[46] Subsequent studies[47,48] reported enhancement of the phosphorescence of ZrO_2 by doping with Ti with the optimum doping level around 0.08 mol %,[47] and it was proposed that the luminescent center is formed by a Ti^{3+} ion that substitutes for Zr^{4+}, and that sixfold O-atom coordination around Ti^{3+} facilitates the formation of a V^{2-} oxygen vacancy.[48] In the more recent literature it has usually been accepted that Ti is the phosphorescence activator in ZrO_2.[49-51] However, it is important to note that the preparation of Ti-doped HfO_2 or ZrO_2 involved high-temperature treatment of the mixtures of starting materials at temperatures exceeding 1200 °C.[44,47,49,51] It is thus possible that the effects of Ti addition and thermal treatment (the latter causing, for example, enhanced crystallinity) were not decoupled in the reported studies, and that phosphorescence activation by intrinsic defects occurred during the thermal treatment. While it is plausible that Ti^{3+} substitutions promote the formation of O vacancies, the vacancies are already present in HfO_2 and ZrO_2, and are thought to be dominant intrinsic defects in these oxides. It has been reported that the TL response of undoped ZrO_2 depends strongly on the degree of crystallinity and, based on this dependence, once again proposed that the luminescent centers as well as charge traps are intrinsic to ZrO_2 and originate from asymmetric coordination of Zr by O atoms.[52,53]

Phosphorescence and TL of polycrystalline HfO_2 samples

Samples for this study were prepared from nominally pure HfO_2 fine powders. The powders were pressed into pellets at room temperature, and some of the pellets were subsequently annealed at 1300 or 1500 °C in inert (Ar) or oxidizing (dry air) atmospheres. The content of Ti impurity in our HfO_2 samples was very low (< 4 ppm), supporting the argument that charge trapping responsible for the phosphorescence is of intrinsic origin. The emission spectrum of the phosphorescence showed a broad band centered at 2.53 eV. The fluorescence spectrum had a very similar shape, with a small (30 meV) blueshift. For annealed samples, the emission was visible to the naked eye for >30 min following excitation at 4.88 eV. Figure 24 shows the phosphorescence time decays for bulk HfO_2 samples. The time-integrated emission intensity ("light sum") for pellets annealed at 1500 °C is more than an order of magnitude higher than that before annealing, indicating that the number of charge traps is significantly increased. Annealing in oxidizing atmosphere causes more intense phosphorescence than annealing in inert gas at the same temperature, although SEM images show that the grain size is independent on the annealing atmosphere. The time decays follow the functional form $\propto (t + t_0)^{-n}$, with parameter n (kinetics order) in the range 1.6-2. This behavior suggests that charge that escapes a trap can be re-trapped with a significant probability.[54,55]

The TL glow curves were measured by cooling a sample to a low temperature, irradiating the sample at this temperature, and subsequently heating it with a linear heating rate while collecting the emitted light. The emission results from radiative recombination of charge carriers that were generated by photoexcitation and captured by trapping centers. In bulk HfO_2, three TL

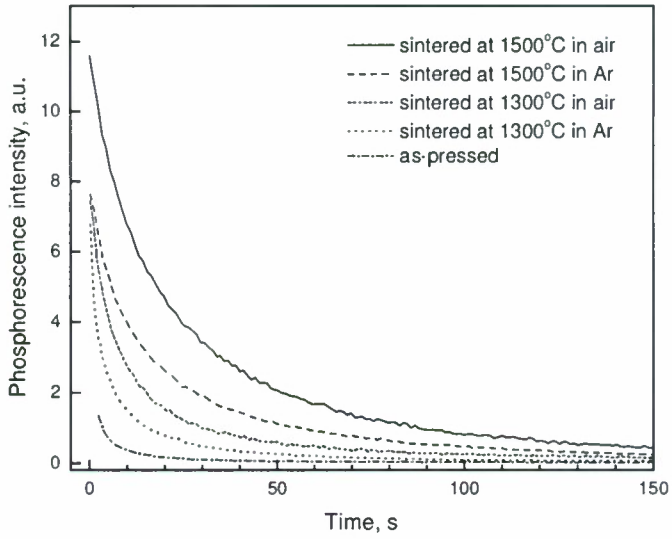

Figure 24. Phosphorescence time dependence for as-pressed and sintered HfO_2 pellets.

peaks are observed in the temperature range ~60-250 °C, and the relative peak intensities strongly depend on the annealing conditions (Fig. 25). The TL curves are qualitatively similar to those reported for pure and Ti-doped ZrO_2.[47-51,53] This similarity *per se* does not indicate that the presence of Ti or some other impurity common to both materials is responsible for the occurrence of charge traps. Given that the two oxides have exceedingly similar crystalline and electronic structures, it is likely that analogous intrinsic defects are formed in both systems, which would also be reflected in similar TL glow curves.

Phosphorescence and TL of PLD HfO_2 films

Experiments have confirmed TL in PLD HfO_2 films on Si (~200 nm thick). A film grown at room temperature and annealed in air at 1350 °C is crystalline and it shows a TL curve similar to those of annealed HfO_2 pellets (Fig. 26a). A film grown at 900 °C has a lower level of crystallinity and shows an order of magnitude lower TL glow intensity and much broader peaks than the annealed film (Fig. 26b). The TL curves of films grown at 25 °C (amorphous) and 700 °C (crystallite size <10 nm), show only a single, very broad TL feature (Fig. 26b). Note that all samples show TL at room temperature, indicating charge trapping under ambient conditions, although the emission is visible by naked eye only for the annealed sample.

The results summarized above demonstrate that the phosphorescence and TL responses of HfO_2, which result from trapping of photogenerated charge carriers, are strongly correlated with the material's microstructure and oxygen content (the latter correlation is indicated by the dependence on annealing atmosphere, given that annealing in Ar should produce a more oxygen-deficient structure). The charge traps are present in the bulk of HfO_2 and seem to be intrinsic in origin, rather than induced by impurities. Further investigation of TL and phosphorescence is required to clarify the origin of charge traps. The observation of phosphorescence with a spectrum that nearly overlaps in energy to that of PL emission suggests that the two types of emission involve the same energy levels, at least one of which must be in the bandgap. Detailed studies of the time dependence of this emission in a broad range of time scales, at different temperatures (such that different types of trapping states are involved), and for samples with

different and well-known microstructures and stoichiometries would help elucidate the trapping mechanisms and sources of charge traps.

As a logical next step in this investigation, the PI attempted to detect phosphorescence and TL from $HfO_{2-x}C_y$ films, both amorphous and those that underwent crystallization. However, no long-living luminescence was detected. The absence of these effects in $HfO_{2-x}C_y$ is probably a result of electrical conduction pathways, introduced by the network of sp^2 carbon, which act to dissipate the photogenerated charge before it undergoes trapping.

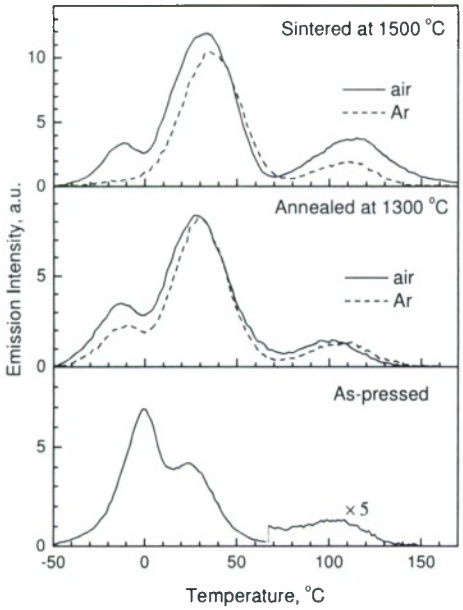

Figure 25. TL glow curves for as-pressed and sintered HfO_2 pellets.

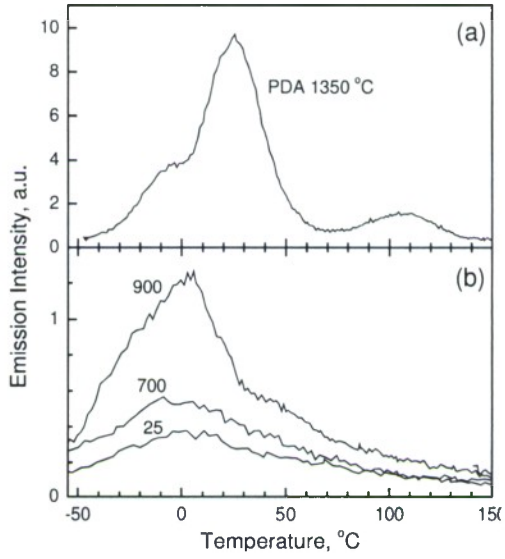

Figure 26. TL glow curves for HfO_2 films: (a) Film annealed at 1350 °C; (b) As-deposited films grown at temperatures (in °C) indicated above curves.

ACKNOWLEDGMENT/DISCLAIMER

This work was sponsored by the Air Force Office of Scientific Research, USAF, under Contract FA9550-07-C-0046. The views and conclusions contained herein are those of the author and should not be interpreted as necessarily representing the official policies or endorsements, either expressed or implied, of the Air Force Office of Scientific Research or the U. S. Government.

ON-SITE PERSONNEL SUPPORTED

Dušan Pejaković Research Physicist, Molecular Physics Laboratory

PUBLICATIONS

D. A. Pejaković, J. Marschall, M. R. George, B. R. Rogers, W. R. Nieveen, and V. Pajcini, "Synthesis of Carbon-Rich Hafnia Thin Films by Pulsed Laser Deposition," *Journal of the European Ceramic Society*, in press (2010).

D. A. Pejaković, "Studies of the Phosphorescence of Polycrystalline Hafnia," *Journal of Luminescence*, in press (2010).

D. A. Pejaković, U. Sharma, "Crystallization Properties of Carbon-Rich Hafnia," in preparation.

INTERACTIONS/TRANSITIONS

During the course of this project, SRI has maintained active collaboration with Vanderbilt University (Prof. Bridget Rogers). In the 2nd and 3rd years of the project, Dr. Pejaković established working collaboration with Evans Analytical Group (Sunnyvale, CA), whose scientists (Vasil Pajcini, Wes Nieveen, Udit Sharma, Bruce Rothman) performed a number of sophisticated analyses of thin film samples. In the 3rd project year, Dr. Pejaković also established active interaction with Prof. Ilke Arslan (UC Davis) related to the studies of the luminescent properties of HfO_2.

The results of this project have led to the following talks/presentations:

"Thin Films of Hafnium-Based Refractory Compounds Synthesized by Pulsed Laser Deposition," poster, UHTC Workshop, July 2007, Menlo Park, CA,.

"Thin Films of Hafnium Oxide with Excess Carbon for High-Temperature Oxidation Protection," invited talk, 2008 AFOSR High Temperature Aerospace Materials Contractors' Meeting, May 12-16, 2008, Vienna, VA.

"Synthesis and Properties of Carbon-Rich Hafnia Thin Films," poster, Ultra-High Temperature Ceramics Conference, 3-8 August 3-8, 2008, Lake Tahoe, CA.

"Carbon-Rich Hafnia Thin Films Synthesized by Pulsed Laser Deposition," poster, AFOSR Workshop on Aerospace Materials for Extreme Environments, 3-5 August 2009, Saint Louis, MO.

DISCOVERIES/INVENTIONS/PATENTS

None.

HONORS/AWARDS

SRI International Service Award, 2007.

REFERENCES

[1]C. B. Bargeron, R. C. Benson, and A. N. Jette, "High-Temperature Diffusion of Oxygen in Oxidizing Hafnium Carbide Films," NASA CP-3054, Part 1, National Aeronautics and Space Administration, Washington, DC, 1989; pp. 83-94.

[2]C. B. Bargeron, R. C. Benson, A. N. Jette, and T. E. Phillips, "Oxidation of Hafnium Carbide in the Temperature Range 1400 ° to 2060 °C," *Journal of the American Ceramic Society,* **76**[4] 1040-46 (1993).

[3]C. B. Bargeron, R. C. Benson, R. W. Newman, A. N. Jette, and T. E. Phillips, "Oxidation Mechanisms of Hafnium Carbide and Hafnium Diboride in the Temperature Range 1400 to 2100 °C," *Johns Hopkins APL Technical Digest,* **14**[1] 29-35 (1993).

[4] (Spectrographic analysis showed that the main impurities in HfO_2 were: Zr (< 0.5%); Zn (0.01%); Si (< 0.002%); and Pb (< 0.01%).).

[5]V. V. Afanas'ev, A. Stesmans, F. Chen, X. Shi, and S. A. Campbell, "Internal Photoemission of Electrons and Holes from (100)Si into HfO_2," *Applied Physics Letters,* **81**[6] 1053-55 (2002).

[6]Y. J. Cho, N. V. Nguyen, C. A. Richter, J. R. Ehrstein, B. H. Lee, and J. C. Lee, "Spectroscopic Ellipsometry Characterization of High-k Dielectric HfO_2 Thin Films and the High-Temperature Annealing Effects on Their Optical Properties," *Applied Physics Letters,* **80**[7] 1249-51 (2002).

[7]M. Balog, M. Schieber, M. Michman, and S. Patai, "Chemical Vapor Deposition and Characterization of HfO_2 Films from Organo-Hafnium Compounds," *Thin Solid Films,* **41** 247-59 (1977).

[8]A. Callegari, E. Cartier, M. Gribelyuk, H. F. Okom-Schmidt, and T. Zabel, "Physical and Electrical Characterization of Hafnium Oxide and Hafnium Silicate Sputtered Films," *Journal of Applied Physics,* **90**[12] 6466-74 (2001).

[9]J. Aarik, H. Mändar, M. Kirm, and L. Pung, "Optical Characterization of HfO_2 Thin Films Grown by Atomic Layer Deposition," *Thin Solid Films,* **466** 41-47 (2004).

[10]T. Ito, M. Maeda, K. Nakamura, H. Kato, and Y. Ohki, "Similarities in Photoluminescence in Hafnia and Zirconia Induced by Ultraviolet Photons," *Journal of Applied Physics,* **97** 054104 (2005).

[11]G. Lucovsky, H. Seo, L. B. Fleming, J. Luning, P. Lysaght, and G. Bersuker, "Studies of Bonding Defects, and Defect State Suppression in HfO_2 by Soft X-Ray Absorption and Photoelectron Spectroscopies," *Surface Science,* **601**[18] 4236-41 (2007).

[12]Z. F. Ren, Z. P. Huang, J. W. Xu, J. H. Wang, P. Bush, M. P. Siegal, and P. N. Provencio, "Synthesis of Large Arrays of Well-Aligned Carbon Nanotubes on Glass," *Science,* **282**[5391] 1105 (1998).

[13]A. de Graaf, M. F. A. M. van Hest, M. C. M. van de Sanden, K. G. Y. Letourneur, and D. C. Schram, "Argon Ion-Induced Dissociation of Acetylene in an Expanding Ar/C_2H_2 Plasma," *Applied Physics Letters,* **74**[20] 2927-29 (1999).

[14]N. G. Shang, F. C. K. Au, X. M. Meng, C. S. Lee, I. Bello, and S. T. Lee, "Uniform Carbon Nanoflake Films and Their Field Emissions," *Chemical Physics Letters,* **358** 187-91 (2002).

[15]H. Okabe, "Photochemistry of Acetylene," *Canadian Journal of Chemistry,* **61** 850-55 (1983).

[16]D. B. Chrisey and G. K. Hubler (Eds.), "Pulsed Laser Deposition of Thin Films." John Wiley & Sons: New York, (1994).

[17]M. Ratzke, M. Kappa, D. Wolfframm, S. Kouteva-Arguirova, and J. Reif, "PLD of High-κ Dielectric Films on Silicon," *Proceedings of SPIE,* **5662** 406-11 (2004).

[18]S. V. Ushakov, A. Navrotsky, Y. Yang, S. Stemmer, K. Kukli, M. Ritala, M. A. Leskela, P. Fejes, A. Demkov, C. Wang, B.-Y. Nguyen, D. Triyoso, and P. Tobin, "Crystallization in Hafnia- and Zirconia-Based Systems," *Physica Status Solidi,* **241**[10] 2268-78 (2004).

[19]L. Zhong, W. L. Daniel, Z. Zhang, S. A. Campbell, and W. L. Gladfelter, "Atomic Layer Deposition, Characterization, and Dielectric Properties of HfO_2/SiO_2 Nanolaminates and Comparisons with Their Homogeneous Mixtures," *Chemical Vapor Deposition,* **12** 143-50 (2006).

[20]N. D. Afify, G. Dalba, U. M. K. Koppolu, C. Armellini, Y. Jestin, and F. Rocca, "XRD and EXAFS Studies of HfO_2 Crystallization in SiO_2-HfO_2 Films," *Materials Science in Semiconductor Processing,* **9**[6] 1043-48 (2006).

[21]S. V. Ushakov, C. E. Brown, A. Navrotsky, A. Demkov, C. Wang, and B.-Y. Nguyen, "Thermal Analyses of Bulk Amorphous Oxides and Silicates of Zirconium and Hafnium," *Materials Research Society Symposia Proceedings,* **745** 3 (2003).

[22]C. Essary, J. M. Howard, V. Craciun, D. Craciun, and R. K. Singh, "Kinetics of Interfacial Layer Formation During Deposition of HfO_2 on Silicon," *Thin Solid Films,* **450** 111-13 (2004).

[23]T. S. Böscke, S. Govindarajan, P. D. Kirsch, P. Y. Hung, C. Krug, B. H. Lee, J. Heitmann, U. Schröder, G. Pant, B. E. Gnade, and W. H. Krautschneider, "Stabilization of Higher-κ Tetragonal HfO_2 by SiO_2 Admixture Enabling Thermally Stable Metal-Insulator-Metal Capacitors," *Applied Physics Letters,* **91** 072902 (2007).

[24]W. J. Zhu, T. Tamagawa, M. Gibson, T. Furukawa, and T. P. Ma, "Effect of Al Inclusion in HfO_2 on the Physical and Electrical Properties of the Dielectrics," *IEEE Electron Device Letters,* **23**[11] 649-51 (2002).

[25]Q. He, H.-B. Guo, J.-J. Wei, S. J. Askari, H.-B. Wang, S.-Y. Zhang, H. Yang, X.-P. Su, and F.-X. Lu, "Deposition of HfO_2 Thin Films on ZnS Substrates," *Thin Solid Films,* **516** 4695-99 (2008).

[26]A. C. Ferrari and J. Robertson, "Interpretation of Raman Spectra of Disordered and Amorphous Carbon," *Physical Review B,* **61**[20] 14095-107 (2000).

[27]F. Tuinstra and J. L. Koenig, "Raman Spectrum of Graphite," *Journal of Chemical Physics,* **53**[3] 1126 (1970).

[28]C. Thomsen and S. Reich, "Double Resonant Raman Scattering in Graphite," *Physical Review Letters,* **85**[24] 5214-17 (2000).

[29]S. N. Tkachev, M. H. Manghnani, A. Niilisk, J. Aarik, and H. Mändar, "Raman and Brillouin Scattering Spectroscopy Studies of Atomic Layer-Deposited ZrO_2 and HfO_2 Thin Films," *Spectrochimica Acta Part A,* **61** 2434-38 (2005).

[30]P. A. Temple and C. E. Hathaway, "Multiphonon Raman Spectrum of Silicon," *Physical Review B,* **7**[8] 3685-97 (1973).

[31]C. Casiraghi, F. Piazza, A. C. Ferrari, D. Grambole, and J. Robertson, "Bonding in Hydrogenated Diamond-Like Carbon by Raman Spectroscopy," *Diamond & Related Materials,* **14** 1098-102 (2005).

[32]J. Robertson, "Recombination and Photoluminescence Mechanism in Hydrogenated Amorphous Carbon," *Physical Review B,* **53**[24] 16302-05 (1996).

[33]A. C. Ferrari and J. Robertson, "Resonant Raman Spectroscopy of Disordered, Amorphous, and Diamondlike Carbon," *Physical Review B,* **64** 075414 (2001).

[34]N. M. J. Conway, A. C. Ferrari, A. J. Flewitt, J. Robertson, W. I. Milne, A. Tagliaferro, and W. Beyer, "Defect and Disorder reduction by Annealing in Hydrogenated Tetrahedral Amorphous Carbon," *Diamond & Related Materials,* **9** 765-70 (2000).

[35]A. Ilie, A. C. Ferrari, T. Yagi, and J. Robertson, "Effect of sp^2-Phase Nanostructure on Field Emission from Amorhous Carbons," *Applied Physics Letters,* **76**[18] 2627-29 (2000).

[36]D. S. Knight and W. B. White, "Characterization of Diamond Films by Raman Spectroscopy," *Journal of Materials Research,* **4**[2] 385-93 (1988).

[37]D. R. Tallant, J. E. Permeter, M. P. Siegal, and R. L. Simpson, "The Thermal Stability of Diamond-Like Carbon," *Diamond & Related Materials,* **4** 191-99 (1995).

[38]S. Shimada, K. Nakajima, and M. Inagaki, "Oxidation of Single Crystals of Hafnium Carbide in a Temperature Range of 600 ° to 900 °C," *Journal of the American Ceramic Society,* **80**[7] 1749-56 (1997).

[39]S. Shimada, F. Yunazar, and S. Otani, "Oxidation of Hafnium Carbide and Titanium Carbide Single Crystals with the Formation of Carbon at High Temperatures and Low Temperatures and Low Oxygen Pressures," *Journal of the American Ceramic Society,* **83**[4] 721-28 (2000).

[40]L. V. Goncharova, M. Dalponte, D. G. Starodub, T. Gustafsson, E. Garfunkel, P. S. Lysaght, B. Foran, J. Barnett, and G. Bersuker, "Oxygen Diffusion and Reactions in Hf-Based Dielectrics," *Applied Physics Letters,* **89** 044108 (2006).

[41]A. S. Foster, F. Lopez Gejo, A. L. Shluger, and R. M. Nieminen, "Vacancy and Interstitial Defects in Hafnia," *Physical Review B,* **65** 174117 (2002).

[42]L. A. Simpson and R. E. Carter, "Oxygen Exchange and Diffusion in Calcia-Stabilized Zirconia," *Journal of the American Ceramic Society,* **49**[3] 139-44 (1965).

[43]G. Knöner, K. Reimann, R. Röwer, U. Södervall, and H.-E. Schaefer, "Enhanced Oxygen Diffusivity in Interfaces of Nanocrystalline $ZrO_2{\cdot}Y_2O_3$," *Proceedings of the National Academy of Sciences,* **100**[7] 3870-73 (2003).

[44]W. J. Schipper, J. J. Piet, H. J. de Jager, and G. Blasse, "On the Luminescence of Hafnium Compounds," *Materials Research Bulletin,* **29** 23-30 (1994).

[45]D. Lim and R. Haight, "Temperature Dependent Defect Formation and Charging in Hafnium Oxides and Silicates," *Journal of Vacuum Science and Technology,* **23**[1] 201-05 (2005).

[46]D. E. Harrison, N. T. Melamed, and E. C. Subbarao, "A New Family of Self-Activated Phosphors," *Journal of the Electrochemical Society,* **110** 23-28 (1963).

[47]J. F. Sarver, "Preparation and Luminescent Properties of Ti-Activated Zirconia," *Journal of the Electrochemical Society,* **113**[2] 124-28 (1966).

[48]P. Iacconi, D. Lapraz, and R. Caruba, "Traps and Emission Centers in Thermoluminescent ZrO_2," *Physica Status Solidi A,* **50** 275-83 (1978).

[49]Y. Cong, B. Li, B. Lei, and W. Li, "Long Lasting Phosphorescent Properties of Ti Doped ZrO_2," *Journal of Luminescence,* **126** 822-26 (2007).

[50]Y. Cong, B. Li, X.-J. Wang, B. Lei, and W. Li, "Synthesis and Optical Property Studies of Nanocrystalline ZrO_2:Ti Long-Lasting Phosphors," *Journal of the Electrochemical Society,* **155**[11] K195-K98 (2008).

[51]M. Akiyama, C.-N. Xu, and K. Nonaka, "Intense Visible Light Emission from Stress-Activated ZrO_2:Ti," *Applied Physics Letters,* **81**[3] 457-59 (2002).

[52]S. C. Chang and C. S. Su, "Direct Thermoluminescence of Sintered ZrO_2 Pellets Induced by Ultraviolet Radiation," *Nuclear Tracks and Radiation Measurements,* **20**[3] 511-16 (1992).

[53]S.-C. Chang and C.-S. Su, "Relationship Between Ultraviolet Radiation Induced Thermoluminescence and Crystalline Structure of ZrO_2," *Radiation Effects and Defects in Solids,* **127** 207-13 (1993).

[54]S. Shionoya and W. M. Yen, "Phosphors Handbook," pp. 91. CRC: Boca Raton, FL, (1999).

[55]W. L. Medlin, "Decay of Phosphorescence in $CaCO_3$, $MgCO_3$, $CaMg(CO_3)_2$, and $CaSO_4$," *Physical Review,* **122**[3] 837-42 (1961).